LBL-15658
Preprint c.2

Lawrence Berkeley Laboratory
UNIVERSITY OF CALIFORNIA

Materials & Molecular Research Division

RECEIVED
LAWRENCE
BERKELEY LABORATORY

MAR 14 1984

LIBRARY AND
DOCUMENTS SECTION

To be submitted to Wear

EROSION OF STEELS IN LIQUID SLURRIES

A.V. Levy and P. Yau

December 1983

TWO-WEEK LOAN COPY

This is a Library Circulating Copy which may be borrowed for two weeks. For a personal retention copy, call Tech. Info. Division, Ext. 6782.

Prepared for the U.S. Department of Energy under Contract DE-AC03-76SF00098

LBL-15658 c.2

DISCLAIMER

This document was prepared as an account of work sponsored by the United States Government. While this document is believed to contain correct information, neither the United States Government nor any agency thereof, nor the Regents of the University of California, nor any of their employees, makes any warranty, express or implied, or assumes any legal responsibility for the accuracy, completeness, or usefulness of any information, apparatus, product, or process disclosed, or represents that its use would not infringe privately owned rights. Reference herein to any specific commercial product, process, or service by its trade name, trademark, manufacturer, or otherwise, does not necessarily constitute or imply its endorsement, recommendation, or favoring by the United States Government or any agency thereof, or the Regents of the University of California. The views and opinions of authors expressed herein do not necessarily state or reflect those of the United States Government or any agency thereof or the Regents of the University of California.

LBL-15658

EROSION OF STEELS IN LIQUID SLURRIES

Alan V. Levy and Paul Yau

Materials and Molecular Research Division
Lawrence Berkeley Laboratory
University of California
Berkeley, California 94720

Research sponsored by the Department of Energy under DOE/FEAA 15 10 10 0, Advanced Research and Technical Development, Fossil Energy Materials Program, Work Breakdown Structure Element LBL-3.5 and under Contract No. DE-AC03-76SF00098

ABSTRACT

The erosion of steels commonly used in piping and containment vessels in coal liquefaction plants was investigated. The jet impingement type of test where coal particle containing liquids is directed at flat specimens was used to determine the erosion rates and mechanism of coal slurry erosion. The effects of steel heat treatments, slurry impingement angles, and other slurry erosion test conditions on erosion rates are discussed. Microscopic analysis was used to determine the mechanism of erosion. Comparisons between liquid-solid particle and gas-solid particle erosion are presented.

INTRODUCTION

The conversion of pulverized coal to liquid fuels and the use of coal directly as a fuel carried in a water or oil liquid both impose erosive forces on the materials that contain the coal-liquid slurry flows. In order to gain an understanding of the erosive nature of coal slurries, a jet impingement tester was developed that can direct a slurry of particles in a liquid carrier through a nozzle against a specimen. This test device has been used to determine the erosion behavior of several types of steels over a range of slurry flow conditions. Metallographic analyses of eroded surfaces were combined with erosion rate measurements to determine what the mechanism of erosion was and how variations in the test conditions affected the erosion behavior. The resulting understanding of the erosion process in slurry flows contributes to the selection and development of alloys for this type of service.

EXPERIMENTAL CONDITIONS

In order to determine the effects of precise variations in slurry flow conditions on the erosion of metals, hard coatings and ceramics, a test device was designed and constructed that directs measured quantities of slurry at flat specimen surfaces positioned at specific angles to the flow direction.[1] In the jet impingement tester (JIT) the exposure time can be varied as can the type of slurry and its impingement conditions of velocity and impingement angle. Quantities of slurry ranging from 1 to 80 gal of selected solids loadings can be passed through the device's nozzle to impinge on the specimen in a single test cycle.

Fig. 1 is a diagram of the JIT with the principal elements designated. The equipment operates by air or inert gas pressurizing of the stirred slurry hold tank, Fig. 2, which forces the slurry through the 3 mm dia nozzle, Fig. 3, into the test enclosure, Fig. 4. The test tank contains a specimen holder, Fig. 5, that positions the specimen under the nozzle, approximately 1/2 inch below the nozzle's exit. The holder can be positioned at any impingement angle and holds flat specimens.

The amount of slurry used in a single exposure is controlled by timing the release of the slurry whose flow rate has been calibrated against the hold tank's pressure level. The on-off valve in the nozzle assembly is used to precisely control the release of the slurry through the nozzle. Reproduceability of the test results from the JIT were determined in a series of 5 tests where 30 wt% -200 mesh coal-kerosene slurry was used to erode 1020 steel at 13m/s and an impingement angle

of α=90°. 18 gallons of slurry was used for each test in an 11 min. exposure. Two of the specimens had a weight loss of 0.7 mg and the other 3 specimens had a weight loss of 0.8mg.

In order to determine the amount of eroding slurry to use in each test, a series of incremental erosion tests was carried out. Fig. 6 shows the results of the test. Steady state erosion was achieved after 18 gallons of slurry impinged on the surface. Therefore, 18 gallons were used in all subsequent tests.

The alloys used in the test series are listed in Table 1. Test specimens 3.2cm x 2.0cm x 0.3cm were prepared and the surfaces to be eroded polished with 400 grit SiC. After exposure to 18 gallons of the 30 wt%, -200 mesh coal-kerosene slurry at 25°C at selected velocities and impingement angles, the specimens were removed from the test chamber, cleaned with soap water and ethyl alcohol and immediately weighed on a balance sensitive to 0.0001gm.

RESULTS

Determining the effect of impingement angle on the erosion of ductile metals is the most sensitive way to study the mechanism of erosion. Fig. 7 shows the classical curve from Finnie's work[2] using SiC particles in an air stream for ductile and brittle materials. It can be seen that ductile materials reach a peak erosion rate around an impingement angle, α, of 20° with a decrease in erosion rate at higher impingement angles. Brittle materials behave differently, reaching a peak erosion rate at α= 90°.

Fig. 8 shows the curve obtained for hot rolled 1018 steel, a ductile metal, eroded by a coal-kerosene slurry at three velocities.

The pattern of erosion v.s. impingement angle is quite different from that shown in Fig. 7. The erosion rate increased with the impingement angle, reaching a peak erosion rate at $\alpha=90^{\circ}$. An intermediate peak of erosion occurred at an angle of $\alpha=45^{\circ}$ at the highest slurry velocity. This pattern of erosion was determined to be consistent for all of the steels tested. The proposed reasons for this marked difference in the effect of impingement angle on erosion of ductile metals between gas-solid particle and liquid-solid particle flows is presented in the discussion.

The effect of velocity on the erosion rates of 1018 steel specimens can be seen in Fig. 9. The velocity exponent, n, varied with the impingement angle, generally decreasing with an increasing angle. It's value is less than that measured in gas-solid particle erosion tests of ductile metals.[2] In other slurry erosion tests in a slurry pot tester[3], it was determined that the velocity exponent was also approximately 2.

Fig. 10 compares the erosion rate curves for mild steel and a low alloy steel, AISI 4340. Both steels were tested in the spheroidized condition. The 4340 steel has a tensile strength of 100KSI and an elongation of 25% in this condition while the 1020 steel has a lower tensile strength of 57KSI and an elongation of 36%. While the shape of the two curves in Fig. 9 are somewhat different in the region of the intermediate peak region, they both have approximately the same erosion behavior at the various impingement angles. This occurs in spite of the marked differences in tensile strength and elongation. The stronger but less ductile 4340 has a higher erosion rate at the lower

impingement angles where the shear forces on the eroding surface are higher and about the same erosion rate as the 1020 steel at the higher impingement angles. It's peak erosion region occurs over a wider range of impingement angles than any of the other alloys tested.

The erosion of 4340 steel in three different heat treatment conditions was carried out over a range of impingement angles at room temperature. The purpose was to determine what the effect of hardness, strength, elongation and microstructure had on the erosion behavior of the steel. Fig. 11 shows the erosion rate curves of the three heat treat conditions plotted against the impingement angle. As in earlier tests with other alloys, the general trend is for the steel to undergo increasing erosion rate with impingement angle with the highest erosion rate occurring at $\alpha=90^{\circ}$ and an intermediate erosion peak occurringin the $\alpha=40^{\circ} - 60^{\circ}$ range.

The major erosion rate difference occurring between the as-quenched and the tempered and spheroidized heat treatments is unlike that which occurs in gas-solid particle erosion of 4340 steel[8] where there was almost no effect of heat treatment on the erosion rate. The difference in elongation between the three heat treated steels does not indicate this property to have a major effect on the erosion rate. If it did, the 200°C temper curve would be much nearer the as-quenched curve. The Charpy impact strength of the as-quenched material and its fracture toughness are both significantly lower for the as-quenched material compared to the 200°C temper conditions.[8] While these properties did not affect gas-solid particle erosion rates, they may affect liquid-solid particle erosion rates. The relatively low

strength and hardness of the spheroidized steel may account for its somewhat higher erosion rate compared to the 200°C temper steel.

The effect of the impingement angle on the erosion of two low chromium steels that are commonly used in chemical process plants are shown in Figs. 12 and 13. The 2 1/4Cr 1Mo steel erosion curve in Fig. 12 follows the pattern of increasing erosion rate with impingement angle with an intermediate peak at approximately $\alpha=45^{\circ}$. Unlike the 1018 steel curve in Fig.8, both the 10 and 20m/s velocity curves have an intermediate peak. The difference in the erosion rates between the two velocities is near constant over the range of impingement angles.

The erosion of 5Cr 1/2Mo steel is shown in Fig. 13. The shape of the curves follow the same general pattern, but the erosion rate at $\alpha=90^{\circ}$ is much closer to the value at the intermediate peak which occurs at $\alpha=45^{\circ}$. The shapes of the curves for each velocity digress at the higher impingement angles. The erosion rates for the two chromium bearing steels are near the same at the lower velocity, but the erosion rates of the 5Cr 1/2Mo steel at 20m/s are consistently lower than those of the 2 1/4Cr 1Mo steel. Both of the low chromium steels had about the same erosion rate as the 1020 steel at a velocity of 10m/s but the 2 1/4Cr 1Mo steel had a higher rate at 20m/s. The effect of the composition and morphology variations in the steels tested only affected their erosion behavior at the higher particle velocity.

Fig. 14 shows the effect of impingement angle on the erosion of 410SS (12Cr steel) at 3 different velocities. The curves have the same pattern as those for 1018 steel shown in Fig. 8. The intermediate peak at 30m/s occurs at $\alpha=60^{\circ}$, considerably higher than the peak for the

1018 steel. The erosion rates at the slurry velocities used also differed from those of the 1018 steel being lower at the lower 2 test velocities and near the same at the highest velocity. The rates were generally lower than those for the 2 1/4 and 5Cr steels, figures, 12 and 13.

Fig. 15 shows the effect of impingement angle on the erosion of two commonly used austenitic stainless steels. While the curves have the same general shape as those of the ferritic steels, they both exhibited a much more distinct intermediate peak, at $\alpha=45^{o}$. Their erosion rates were less than those of the ferritic steels, particularly at the intermediate peak impingement angle and higher. The intermediate peak erosion rate was the same as the $\alpha=90^{o}$ rate for both steels.

In order to determine the effect of the liquid's viscosity and the particles' strength on the erosivity of the coal-kerosene slurry, a slurry was prepared of a lower viscosity liquid, water, and a higher strength particle, SiO_2. The SiO_2 particles had a finer particle size, 44μm average dia compared to 74μm average dia for the coal. The coal-kerosene and SiO_2-water slurries were used to erode 1018 plain carbon steel in the spheroidized and hot rolled conditions, respectively. The difference in properties of the two materials is not significant for the purpose of the tests. the resulting curves are shown in Fig. 16. Note the break in the scale on the ordinate. The SiO_2-water slurry caused more than 10 times the erosion of the higher viscosity, lower particle strength, coal-kerosene slurry. The pattern of the curve was the same as all other slurry test results with the intermediate erosion

peak of the SiO_2-water slurry at $\alpha=50^o$ and the peak for the coal-kerosene slurry at $\alpha=40^o$.

A further comparison was made of erosion rates using fluids of a still wider range of effective viscosity by testing 1018 mild steel specimens at the same flow conditions using coal-kerosene in one test and coal char-air in another test. Coal char is somewhat more erosive than coal; it was used instead of coal because the clumping tendency of the coal particles prevented them from flowing out of the hopper in the air-solid particle erosion tester. Both the coal and the char have considerable lower erosivity than particles such as sand or alumina. The particle sizes of the coal and the char were approximately the same, near 100μm dia. The tests were performed at a velocity of 30m/s and an impingement angle of 90° at 25^oC. The air-coal char erodent stream resulted in an order of magnitude higher erosion rate, 4.6×10^{-6}g/g than the coal-kerosene erodent stream which caused an erosion rate of 2.0×10^{-7} to occur.

Microscopic Analysis

Microscopic examination of the eroded surfaces of ductile metals after exposure to small, solid particles carried in either liquid or gas streams show the same mechanism to have taken place. However, the degree of surface deformation differs markedly between gas and liquid-solid particle erosion. The deformation resulting from slurry impingement is much less severe than that which occurs as the result of gas-solid particle impingement. There are also other appearances differences that will be discussed.

Fig 17 shows the surface of a 1020 steel specimen that has been eroded to a steady state condition by 140μm silicon carbide particles carried in an air stream at a velocity of 30m/s and an impingement angle of 30° at 25°C. The surface is covered with distressed platelets that have been extruded-forged by the impacting particles[3]. It is severely deformed as is typical for eroded surfaces of ductile metals in gas-solid particle erosion. Compare the eroded surfaces of Fig. 17 with that of 1020 steel specimen eroded by a 30 wt% coal-kerosene slurry shown in Fig. 18. The lower photo in Fig. 18 is at the same magnification as Fig. 17. The slurry was directed at the test surface from a nozzle at a velocity of 15m/s and an angle of α=30°. The liquid-solid particle eroded surface has undergone markedly less deformation. The few larger marks on the surface that show some platelet formation were probably made by large particles of mineral oxide that were not cleaned or screened out of the -200 mesh coal that was used to make the slurry.

The unique appearing small impressions that occur in clusters on eroded 304SS (Fig. 19) are indicative of what part of the coal is the erosive. Coal itself is too weak to erode steels at a measurable rate in the type of test used in this investigation. It is the mineral content of the coat that has the particle integrity to deform a metal surface when it strikes it. Fig. 20, from the Kentucky Institute for Mining and Mineral Research[4], shows that the small, patterned impressions in the steel, lower photo, are very similar in shape and size to a grouping of pyrite, framboidal clusters that occur in coal particles (top photo). Thus, the coal acts somewhat as a tool holder

to maintain the position of the framboidal erosive as it impacts the metal surface. This phenomena is shown at several locations over the metal surface in Fig. 19.

More of what the nature of the surface deformation is in the erosion process in slurry flows can be determined by studying cross sections of eroded surfaces. The mild nature of the surface deformation, however, makes it very difficult to maintain the structure of the eroded surface through the metallographic cutting and polishing steps. Extra care must be taken in the metallographic preparation of specimens. Fig. 21 shows the cross section of an eroded surface of mild steel. Very thin platelets can be seen extending ahead of shallow craters from which they were extruded by the action of the impacting particles. Part of the platelet on the far left has been broken off by a particle impact, which probably also caused the crack that occurred further back in the platelet. It can be seen that the platelets do not bond to the base metal over which they are extruded. Unlike the type of deformation of the platelets that occurs in gas-solid particle flows in which they extend out from the surface at many angles, the lubricating nature of the kerosene in the coal-kerosene slurry results in a platelet orientation that parallels that of the eroding surface.

Fig. 22 shows the inner eroded surface of a 316SS elbow that was tested in a coal-kerosene slurry loop test system. Its visual surface smoothness belies the fact that erosion was occurring by platelet formation along the surface. Comparing Figs. 21 and 22, leads to the observation that the polished appearance of an eroding surface is

probably due to the platelets that are formed being parallel to the eroding surface.

DISCUSSION

The principal differences between the erosion of ductile metals in gas-solid particle streams and liquid-solid particle slurries are the rate of erosion and the effect of the impingement angle of the particle on the target surface. The erosion rates of ductile metals for the same type and size of eroding particles at the same flow velocities are an order of magnitude higher for gas-solid particle streams than for liquid-solid particle slurries.

The highest rate of erosion occurs at a shallow angle of impingement for metals eroded by gas-solid particle streams while for liquid-solid particle streams the highest erosion rate occurs at an impingement angle of 90° with a lower peak occurring in the 40° - 60° angle range for many, but not all alloys (see Figs. 8 - 16). Both of these major differences may be considered as due to the barrier nature of the liquid carriers impeding the impact of the solid particles on the target metal surfaces.

While the analytical modelling to describe these differences remains to be developed, the physical concepts that account for the differences are known well enough to be discussed. The two properties of the liquid that account for the barrier effect in slurries are their viscosity and lubricity. The viscosity effect was determined in early work[6] and is shown in Fig. 23. It can be seen that the erosion rate was reduced by one order magnitude by using the SRC-1 process solvent instead of water to erode A53 mild steel. The same order of magnitude

difference was observed in the test results plotted in Fig. 16 although some of the latter difference was due to the difference in the erosivity between the coal and sand particles used in these tests.

The effect of lubricity is a somewhat more elusive property to relate to the erosion process, but a successful direct comparison was made in tests using hexadecane, a long chain hydrocarbon, and a version of it which contained 1/2% of its acid. The acid addition did not change the viscosity of the liquid but did change the polarity of the hydrocarbon, increasing its lubricating qualities. The results of this work are shown in Fig. 24 taken from reference 3. The erosion rate of A53 mild steel from the plain hexedecane-coal slurry was almost 3 times that of the same slurry with the small acid addition.

How the effect of the liquid carrier fluid changes the shape of the erosion rate-impingement angle curve as compared to the curve for gas-solid particle erosion, Fig. 7, can be speculated upon in the following manner. At shallow impingement angles, the force of the eroding particles is reduced by the viscous, lubricating film of the carrier fluid that is positioned between the particles and the eroding surface. As the impingement angle increases, the particle momentum can more readily penetrate the barrier film of the liquid and the erosion rate increases. At an impingement angle of 90° the particles are least effected by the lubricating nature of the liquid and transmit a maximum impact force to the target surface. Thus, the highest erosion rate occurs at 90°. Work will be undertaken to mathematically define the

effective forces transmitted to the eroding metal surface for the cases of gas and liquid-solid particle erosion media.

The secondary, lower than maximum erosion rate peak that occurs on the steel alloys tested at impingement angles between 40° and 60° can also be related to the lubricating qualities of the carrier fluid. In gas-solid particle erosion the amount of initial platelet extrusion and further extension by subsequent particle impacts is enhanced by the direction of the applied force of the particles[4]. At shallow impingement angles, between 20° and 30°, the effect of the vertical force component of the eroding particle that extrudes the metal beneath it is maximized by the horizontal component of the force which cause the extrusion to occur out from the point of impact, near parallel to the surface. This results in larger platelets which, in turn, cause greater erosion rates to occur at the peak erosion impingement angles.

In the case of the liquid-solid particle slurries, the lubricating quality of the fluid decreases the eroding force at the shallower angles around 20° - 30°. However, the basic effect of the direction of the applied force enhancing the formation of larger platelets still holds true and a secondary peak still occurs but at an impingement angle that is moved to higher angles, in the 40° - 60° range. Thus, the occurrence of a peak erosion rate effect that is observed in gas-solid particle erosion at shallow angles also occurs in liquid-solid particle erosion, but at greater angles. It's absolute value, however, is mitigated by the lubricating nature of the carrier fluid and it to the 90° impingement angle peak where the erosive ability of the impacting particles are at their maximum.

Another aspect of the effect that the lubricating nature of the liquid carrier has on erosion by slurries is shown in Fig. 8. At the two lower velocities, 10 and 20m/s, the 1018 steel has essentially no intermediate peak. However at the highest velocity used, 30m/s, an intermediate peak does occur. Apparently at the lower velocities the impact force is low enough that the lubricating nature of the liquid overcomes the effect of the distribution of the impacting force and there is little, if any enhancement of the formation of platelets. At the highest velocity, the force becomes great enough to affect the formation of the platelets. 410SS showed the same effect, see Fig. 14.

The effect of the ductility of the target steel on its erosion rate is shown in Fig. 10, which compares 4340 low alloy steel and 1020 steel. For the impingement angles up to 60° the lower ductility but stronger 4340 steel has a somewhat higher erosion rate than the higher ductility 1020 steel. This effect of increasing ductility reducing the erosion rates of steels was reported in Refs. 7 and 8 for gas-solid particle erosion. The effect, then, also occurs in liquid-solid particle erosion, but to a lesser degree. At the higher impingement angles in the liquid slurries where the effect of the lubricating aspect of the fluid is the least, the increased force of the particles on the target material appears to overcome the effect of the difference in ductility and the erosion of the two metals is essentially the same.

This effect relates to the remaining ductility in the plastically deformed platelets. At the lower impingement angles in slurry erosion, it requires more impacts on the formed platelets of the more ductile 1020 steel to finally fracture and remove them, resulting in a lower

erosion rate. At the higher angles of impingement, above 60°, the platelets formed in both the 1020 and 4340 steel alloys are nearer their ultimate elongation upon formation and both alloys thereby produce platelets of the same vulnerability to being fractured and removed by subsequent impacts.

Another comparison between gas-solid particle and liquid-solid particle erosion is possible as the result of the data contained in Fig. 11. It shows that the low ductility 4340 as-quenched steel (8% elong.) has a much higher rate of erosion than the more ductile 200°C temper conditions (11% elong.) and the still more ductile spheroidized annealed 4340 steel (25% elong.). However, the higher ductility spheroidized steel tested had a higher rate of erosion than the less ductile 200°C temper material. Reaching a peak effectiveness in having increased ductility in an alloy result in a lower erosion rate with further increases in ductility (at the expense of strength) reversing the trend was observed and is described in Ref. 7, 8 for gas-solid particle erosion.

The microscopic analysis of the surfaces eroded by liquid-solid particle slurries indicated that the same basic mechanism of erosion occurs in both gas and liquid-solid particle erosion of ductile metals. The formation, extension, and subsequent breaking off of highly distressed platelets in gas-solid particle erosion is discussed extensively in reference 4. The excellent example of the same mechanism occurring in liquid-solid particle erosion shown in Fig. 21 is the logical extension of the gas-solid particle work.

Even though the erosion rate and impingement angle effects between the two types of carrier fluids are markedly different, the same type of transfer of force from the particle to the eroding ductile metal occurs, and thus, the same mechanism of surface deformation and resulting erosion occurs. The effect of velocity on the erosion rate in slurry erosion also relates to the transfer of force from the impacting particle to the surface. The velocity exponent of 2 or less shown in Fig. 9 and reported in Ref. 3 for coal-kerosene slurries in the slurry pot type of erosion test relates to the kinetic energy of the impacting particles, $KE=1/2mv^2$. The lubricating nature of the liquid media changes the nature of the extrusion process primarily by causing the platelet to extend more parallel to the metal surface and in a thinner cross section.

The carbonaceous component of coal is a relatively soft material with a hardness of 294VHN for bituminous coal. Because of this, it's erosivity is relatively low. In Ref. 9, the effect of particle hardness on erosivity in gas-solid particle erosion is discussed. Comparing the hardness of coal as an erodent with that of the weak erodent apatite (300VHN) reported in Ref. 9, it can be surmised that the main bulk of the coal particle is not very erosive. However, coal contains many forms and sizes of much harder mineral matter, such as SiO_2 (700 - 1500VHN) and Al_2O_3 (1900VHN) which are very effective erodents. In the discussion of Figs. 17 - 20 the role of the hard mineral particles in the coal that are primarily responsible for the eroded material loss is presented. Improvements in coal cleaning methods to remove the mineral ash for other reasons will also have a

significant effect on reducing the erosivity of coal in slurry environments.

The selection of low chromium content steels for process equipment applications in coal liquefaction systems are primarily done on the basis of their corrosion resistance and their low elevated temperature strength. The effect of the chromium content of these steels on their erosion, as shown in Figs. 12 and 13, can also be significant, particularly at the higher velocities used in this test program.

CONCLUSIONS

1. Maximum erosion of steels in liquid-solid particle slurry flows occurs at an impingement angle of 90° with a secondary peak erosion occurring at impingement angles of 40° - 60° in some alloys.

2. The viscosity and lubricity of the liquids in slurries reduces the erosivity of their solid particles by an order of magnitude compared to the erosivity of the same kind of particles in a gas stream.

3. The same platelet mechanism of erosion occurs in both gas and liquid-solid particle erosion. The viscosity and lubricity of the liquid orients the platelets formed more parallel to the eroding surface and makes them thinner than occurs when a gas stream carries the erodent particles to the metal surface.

4. Greater ductility generally results in lower erosion rates in low

alloy steels in coal-solvent slurry erosion. Variations in the strength of the steels have a minor effect on erosion rates.

5. The mineral constituents in coal are primarily responsible for the erosion of ductile metals by coal-solvent slurries. Lower ash content coals should cause lower erosion rates to occur in ductile metals.

REFERENCES

1. Li, S., Humphrey, J., Levy, A., "Erosive Wear of ductile metals by a Particle-Laden High Velocity Liquid Jet," Wear 73 No 2, pp. 295-310, November 1981.

2. Finnie, J., "Erosion of Surfaces by Solid Particles," Wear 3, 1960

3. Levy, A. and Hickey, G., "Surface Degradation of Metals in Simulated Synthetic Fuels Plant Environments," NACE, Corrosion 82, paper No. 154, Houston, Texas, May 1982.

4. Levy, A., "The Erosion of Metal Alloys and Their Scales," proceedings of Conference on Corrosion-Erosion-Wear of Materials in Emerging Energy Systems, pp. 298-376, Berkeley, California, January 1982.

5. Sargent, G., Spencer, D., Seques, A., "Slurry Erosion of Materials," proceedings of Conference on Corrosion-Erosion-Wear of Materials in Emerging Energy Systems, pp. 196-231, Berkeley, California, January 1982.

6. Levy, A., "Erosion/Corrosion of Materials in Coal Liquefaction Environments," NACE-Materials Performance, V19, No.11, pp. 45-51, November 1980.

7. Levy, A., "The Solid Particle Erosion Behavior of Steel as a Function of Microstructure," Wear 68 No. 3, pp. 269-288, May 1981.

8. Levy, A., and Foley, T., "The Effect of Heat Treatment on the Erosion Behavior of Steels," proceedings of ASME International Conference on Wear of Materials - 1983, Reston, Birginia, April 1983.

9. Levy, A. and Chik, P., "The Effects of Erodent Composition and Shape on the Erosion of Steel," Report no. LBL-15242, Lawrence Berkeley Laboratory, University of California, Berkeley, California 94720.

TABLE 1

ALLOY COMPOSITION AND CONDITION

ALLOY	COMPOSITION (nominal)								CONDITION
	Cr	Ni	Mo	Si	Mn	C	P/S max	Fe	
1018-1020					0.5	0.2	0.09	bal	hot rolled spheroidized
4340	0.8	1.8	0.3	0.3	0.7	0.4	0.8	bal	as-quenched 200°C temper spheroidized
2 1/4Cr 1Mo	2.2		0.9	0.3	0.4	0.2	0.02	bal	annealed
5Cr 1/2Mo	5.1		0.6	0.02	0.5	0.1	0.02	bal	annealed
410SS	12			1.0	1.0	0.2	0.1	bal	annealed
304SS	18	9		1.0	2.0	0.1	0.1	bal	as-rolled
321SS	18	10	0.4 (Ti)	1.0	2.0	0.1	0.1	bal	as-rolled

TABLE 2

1018 STEEL EROSION RATES IN GAS AND LIQUID-PARTICLE STREAMS

PARTICLE	FLUID	EROSION RATE	TEST CONDITIONS
Coal	Kerosene	$2x10^{-7}$g/g	V=30 m/s for coal and char
Sand	Water	$6x10^{-7}$g/g	V=12 m/s for sand -=90°
Coal Char	Air	$4x10^{-6}$g/g	150-m particles

Figures

Fig. 1. Diagram of jet impingement tester (JIT).

Fig. 2. Slurry hold tank of JIT.

Fig. 3. Jet nozzle of JIT with on-off control valve.

Fig. 4. Test enclosure tank of JIT.

Fig. 5. Specimen holder in JIT test enclosure tank.

Fig. 6. Incremental erosion test of 1020 steel.

Fig. 7. Effect of impingement angle on the gas-solid particle erosion of ductile and brittle materials.

Fig. 8. Effect of impingement angle and velocity on erosion rate of hot rolled 1018 steel.

Fig. 9. Effect of velocity on erosion rate of hot rolled 1018 steel.

Fig. 10. Effect of impingement angle on erosion of spheroidized 1020 and 4340 steels.

Fig. 11. Effect of impingement angle on 4340 steel at 3 heat treatments.

Fig. 12. Effect of impingement angle on erosion of 2 1/4Cr1Mo steel

Fig. 13. Effect of impingement angle on erosion of 5Cr 1/2Mo steel.

Fig. 14. Effect of impingement angle and velocity on erosion of 410SS.

Fig. 15. Effect of impingement angle on erosion of austenitic stainless Steels.

Fig. 16. Effect of impingement angle on the slurry erosion of 1018 steel from coal-kerosene and SiO_2-water slurries.

Fig. 17. Eroded surface of 1020 steel from SiC-air test.

Fig. 18. Eroded surface of 1020 steel from coal-kerosene slurry test.

Fig. 19. Eroded surface of 304SS from coal-kerosene slurry test.

Fig. 20. Pyrite crystallites in coal and impression in eroded steel.

Fig. 21. Cross section of eroded A 53 mild steel specimen.

Fig. 22. Surface of eroded stainless steel elbow.

Fig. 23. Effect of viscosity on the erosion rate of A53 mild steel.

Fig. 24. Effect of lubricity on the erosion rate of A 53 mild steel.

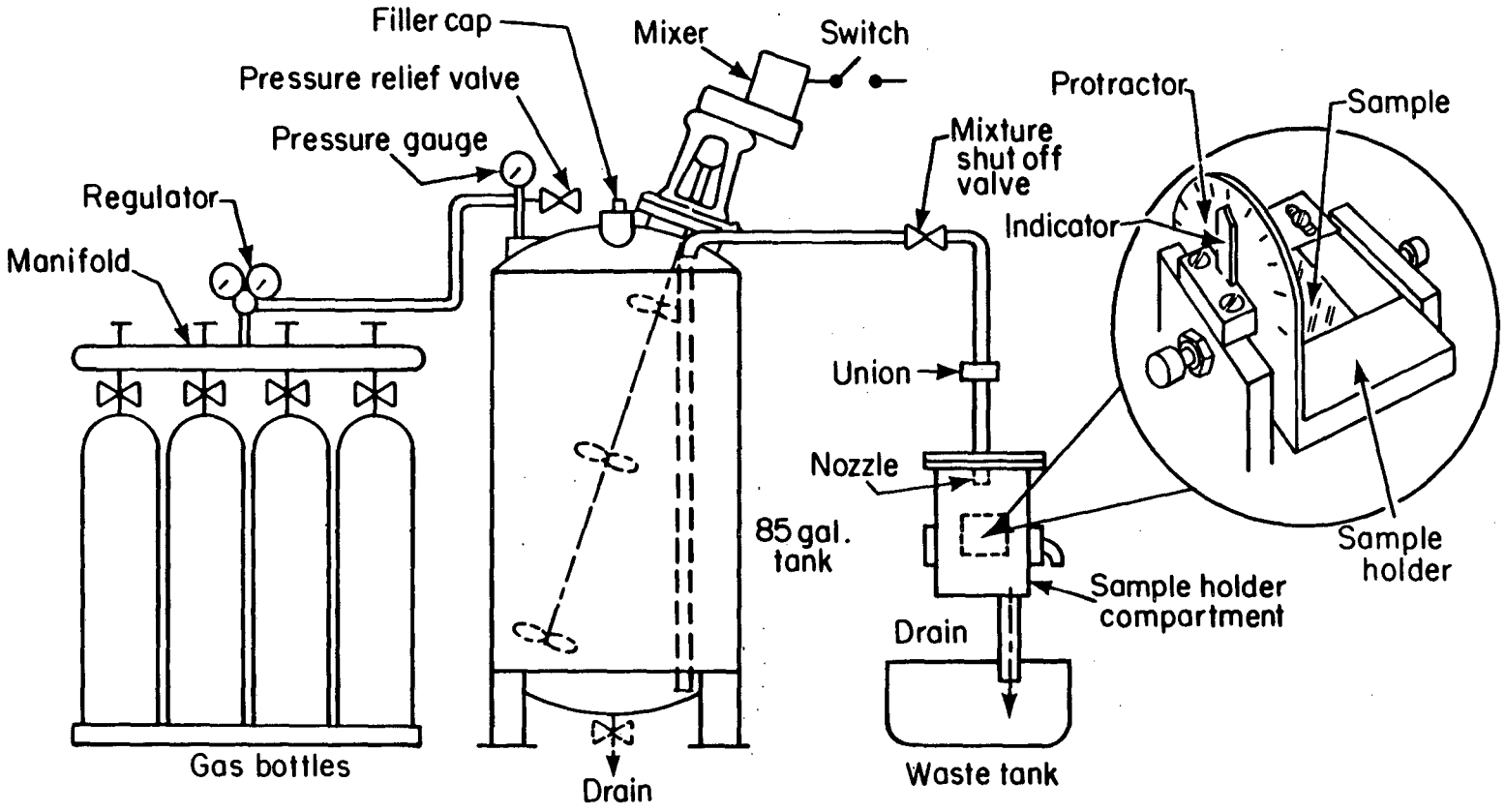

Fig. 1. Diagram of jet impingement tester(JIT)

XBL 816-932

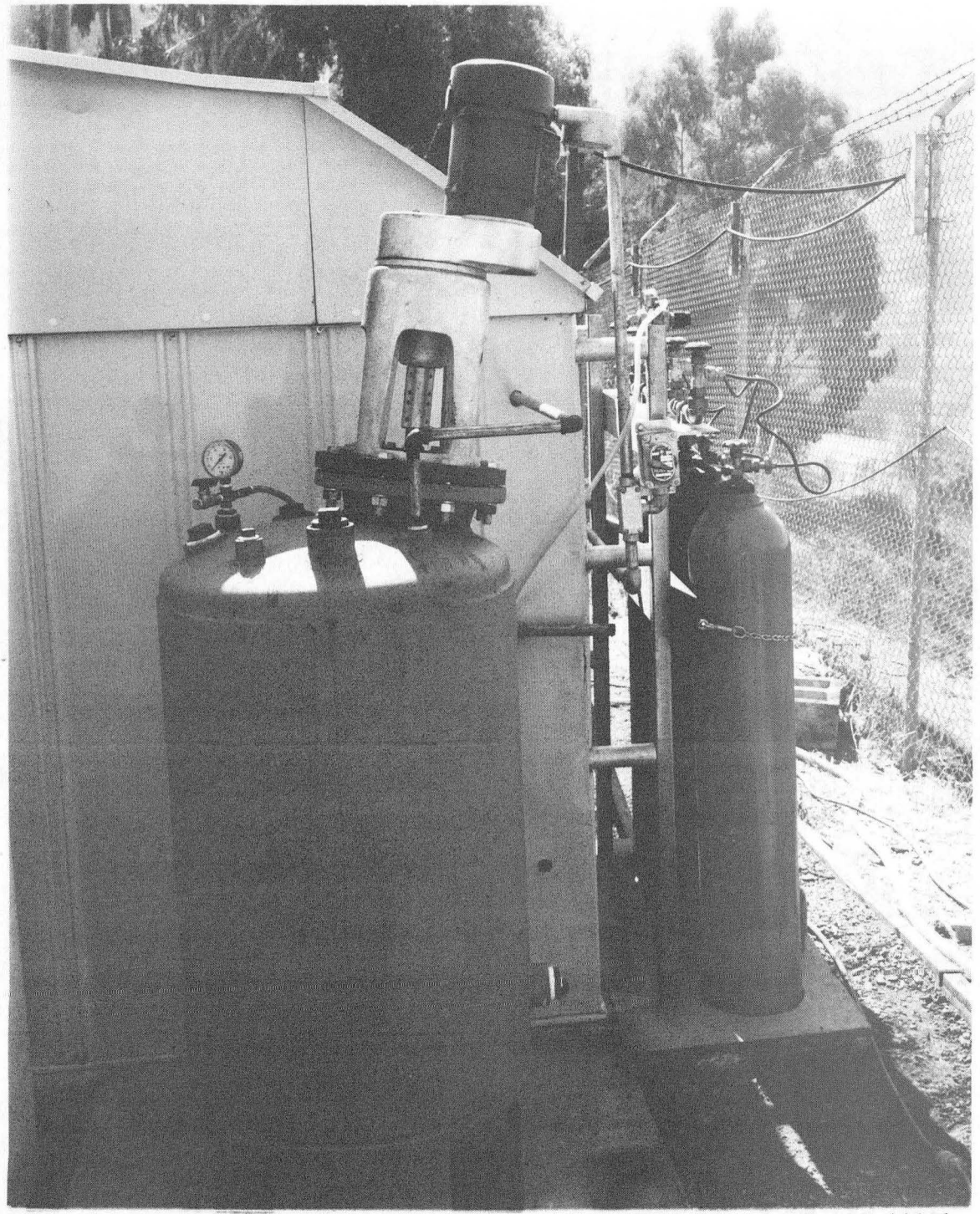

XBB 809-11121

Fig. 2. Slurry hold tank of JIT

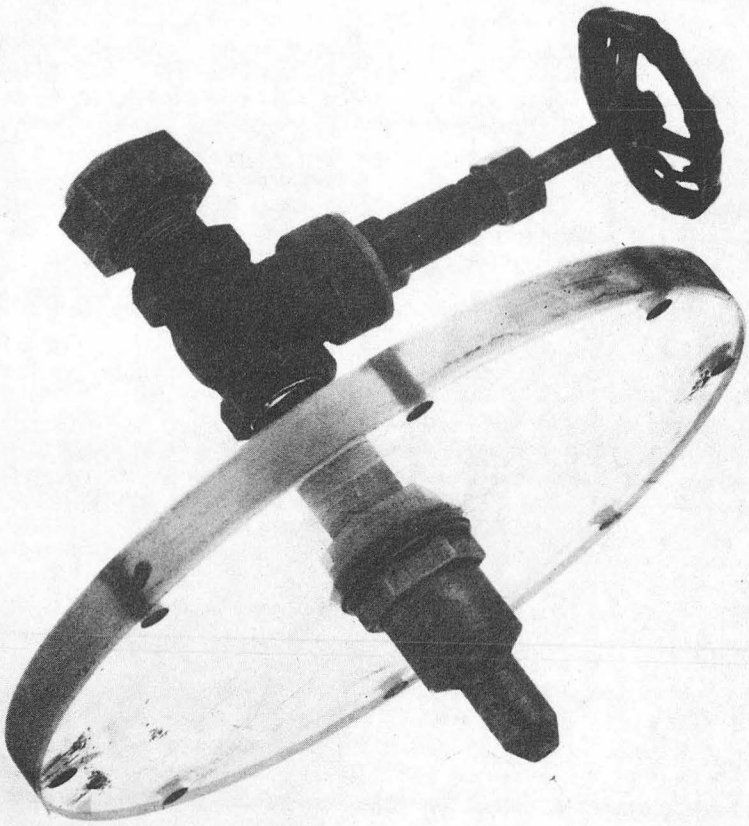

Fig. 3. Jet nozzle of JIT with on-off control valve

XBB 809-11115

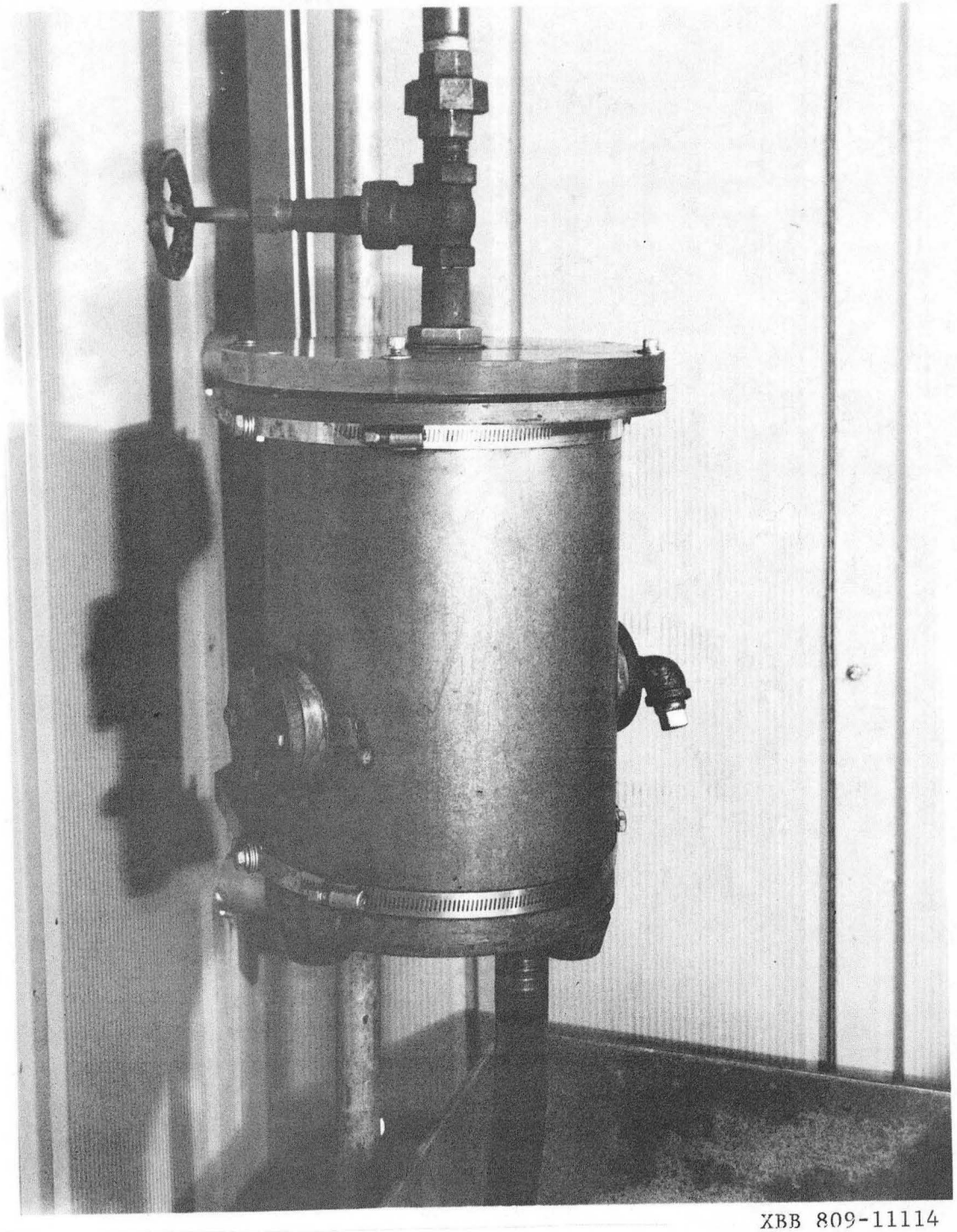

XBB 809-11114

Fig. 4. Test enclosure tank of JIT

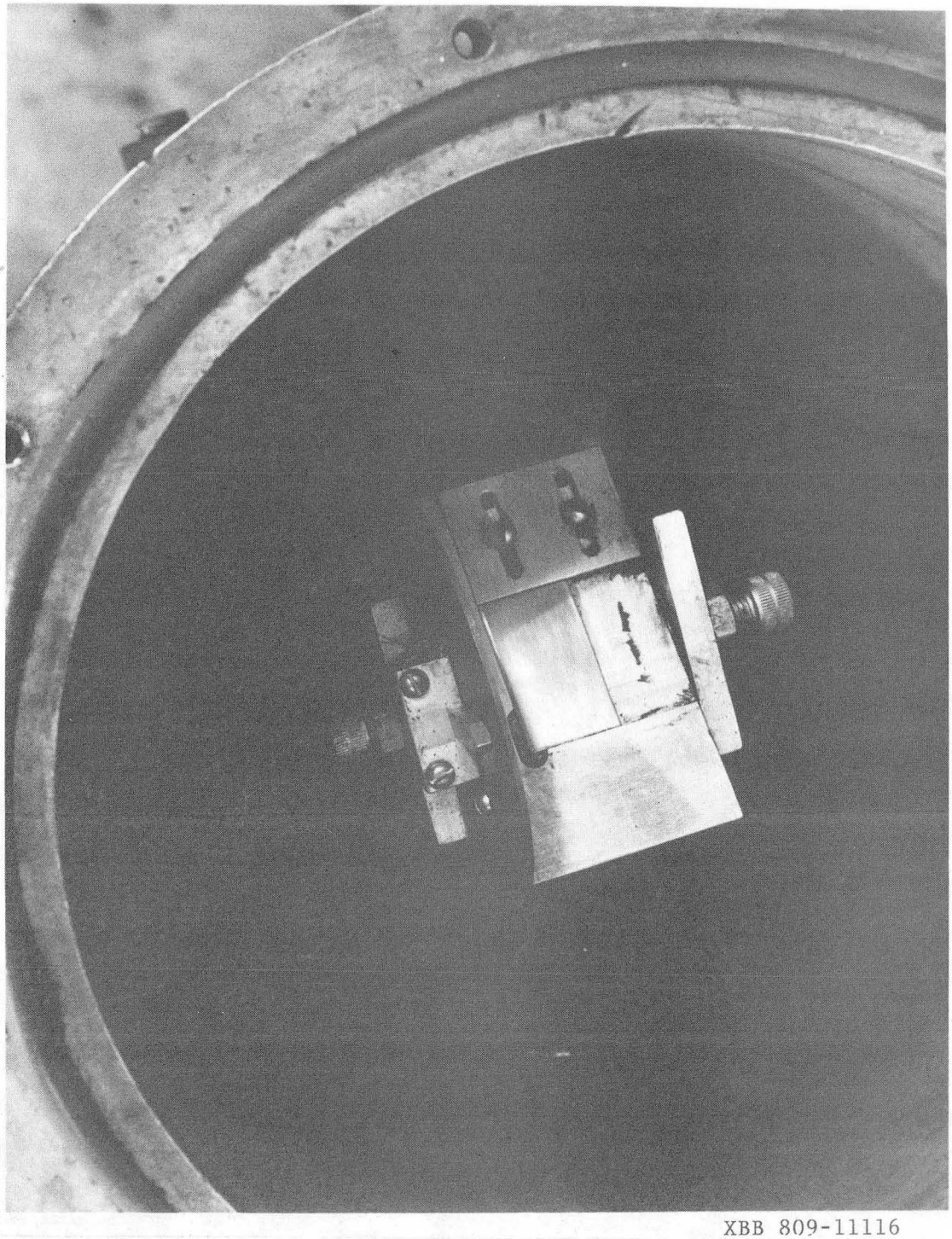

XBB 809-11116

Fig. 5. Specimen holder in JIT test enclosure tank

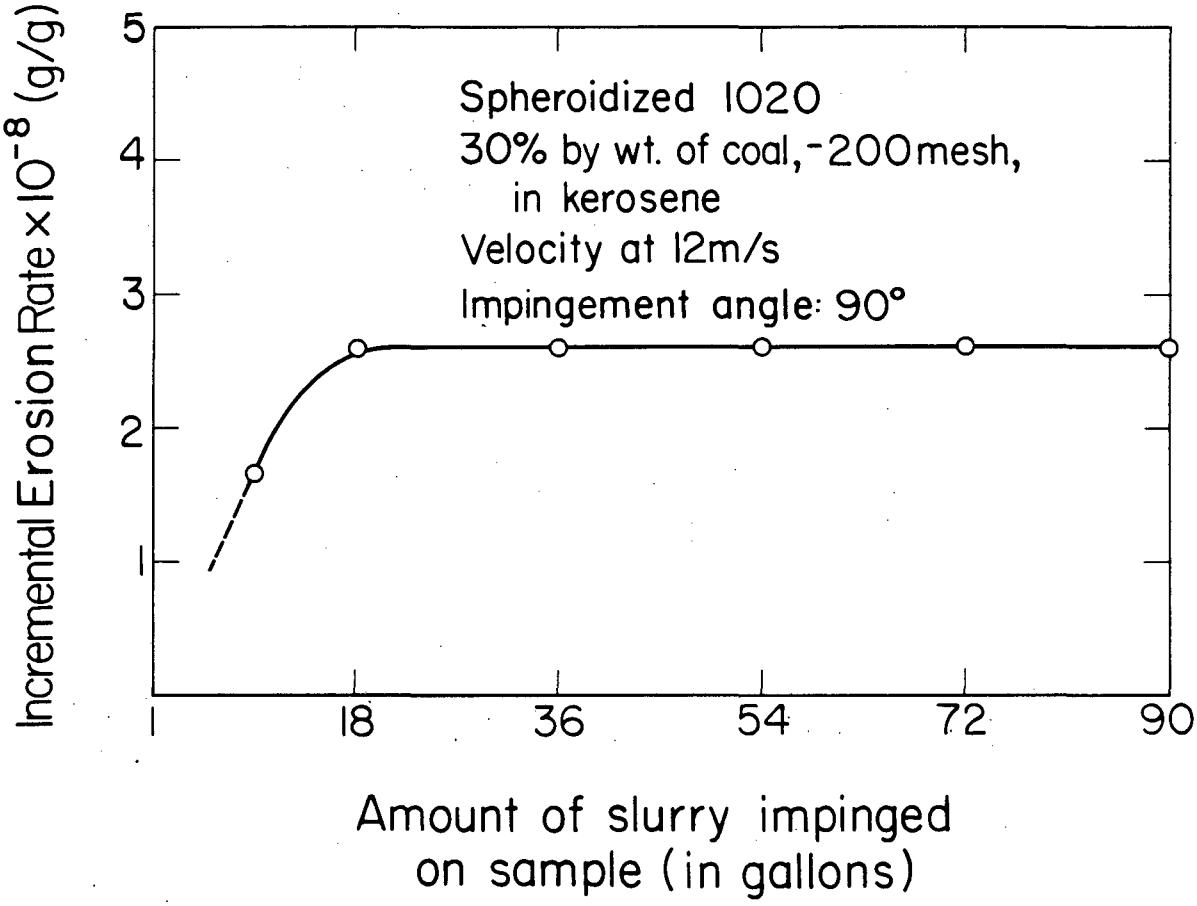

XBL 8110-7142 B

Fig. 6. Incremental erosion test of 1020 steel

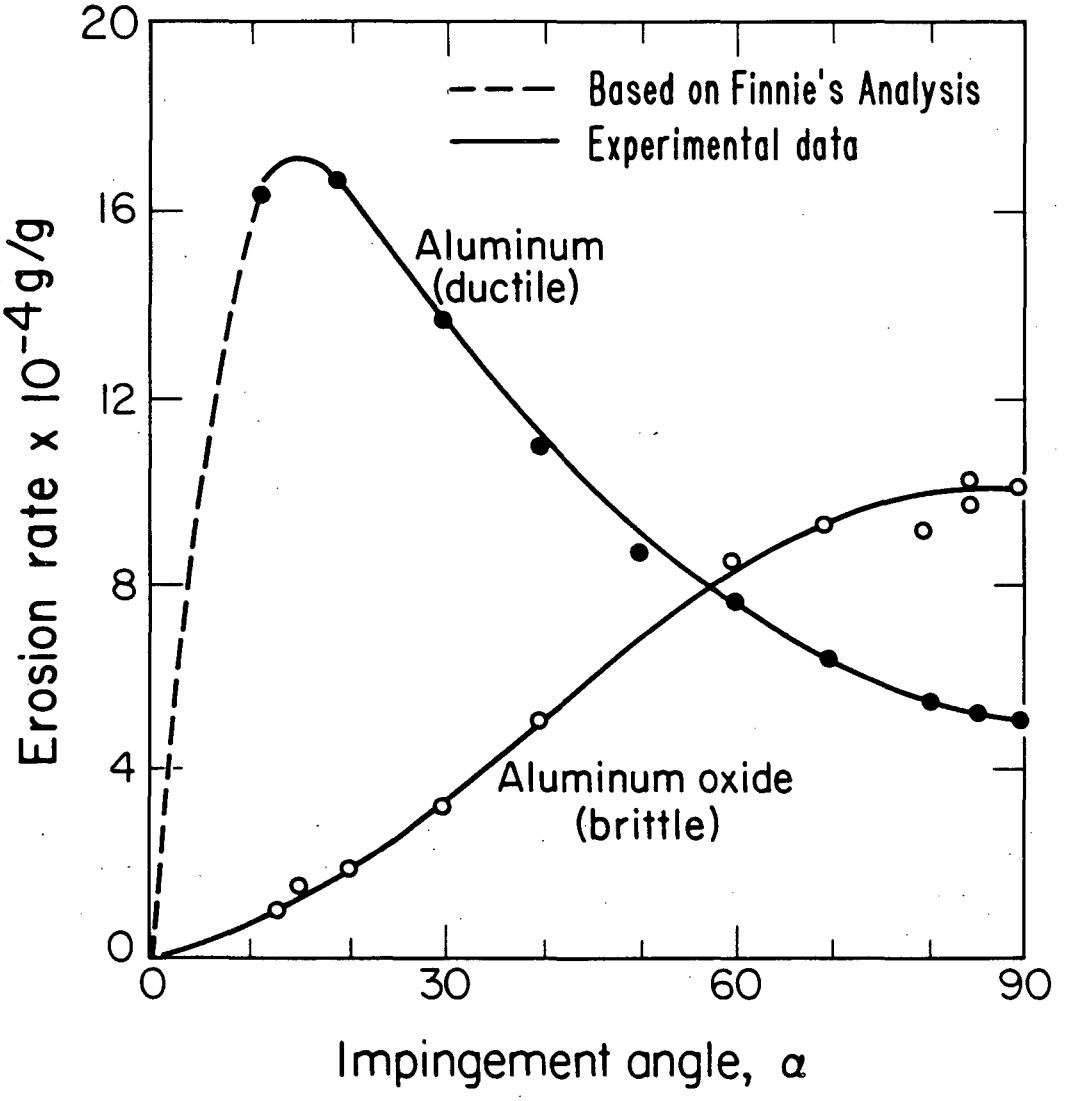

XBL 793-974

Fig. 7. Effect of impingement angle on the gas-solid particle erosion of ductile and brittle materials

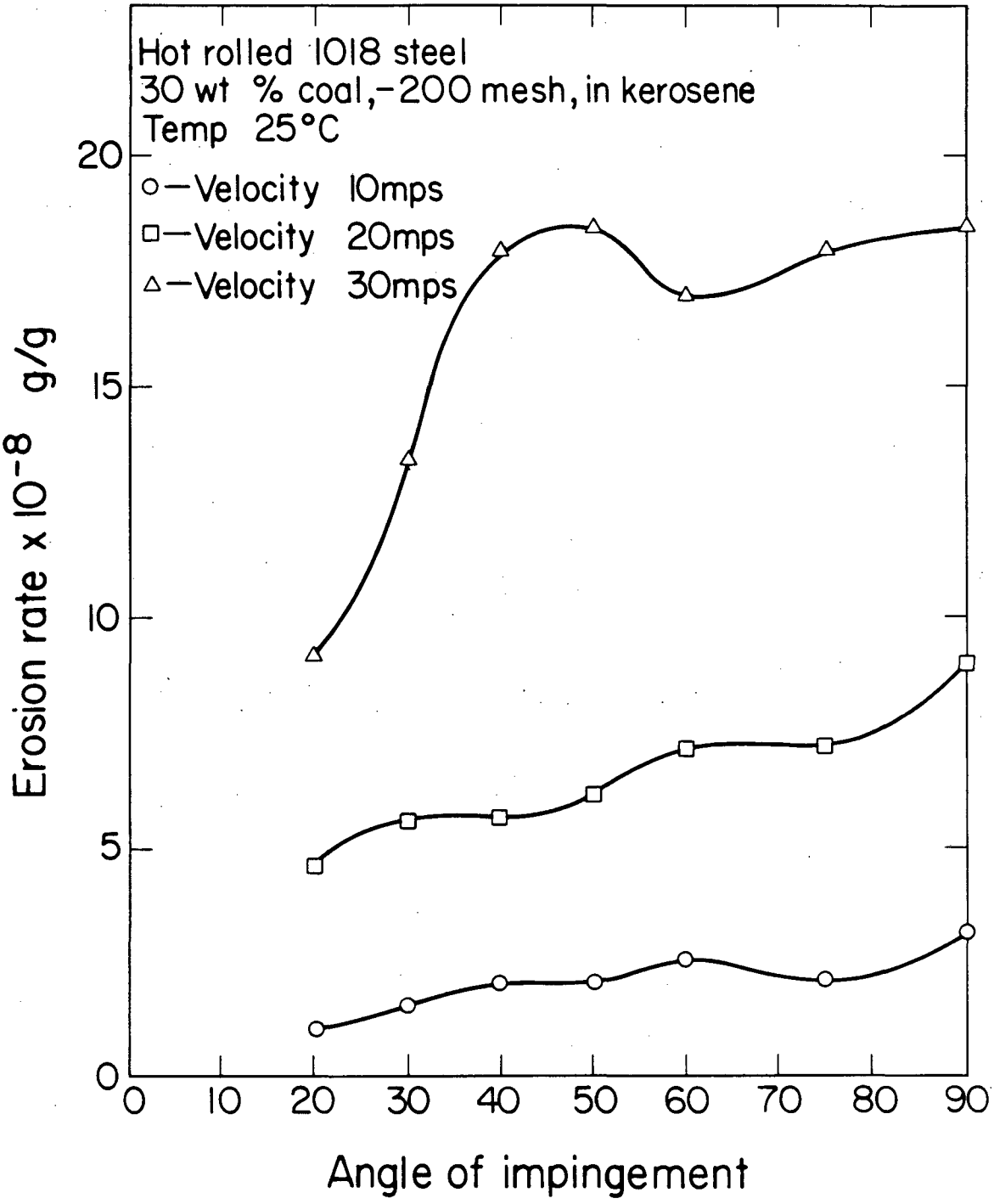

XBL 831-1075

Fig. 8. Effect of impingement angle and velocity on erosion rate of hot rolled 1018 steel

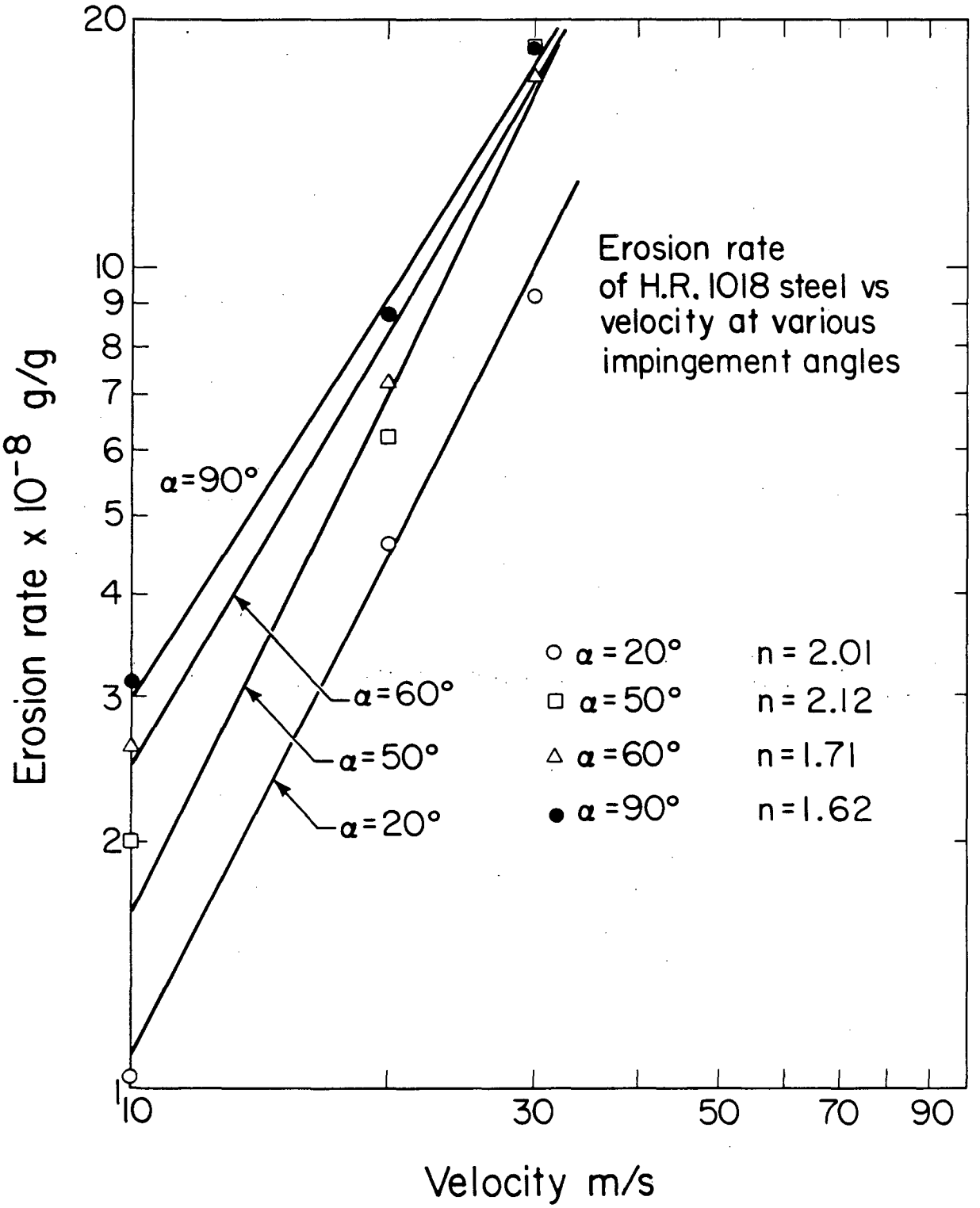

Fig. 9. Effect of velocity on erosion rate of hot rolled 1018 steel

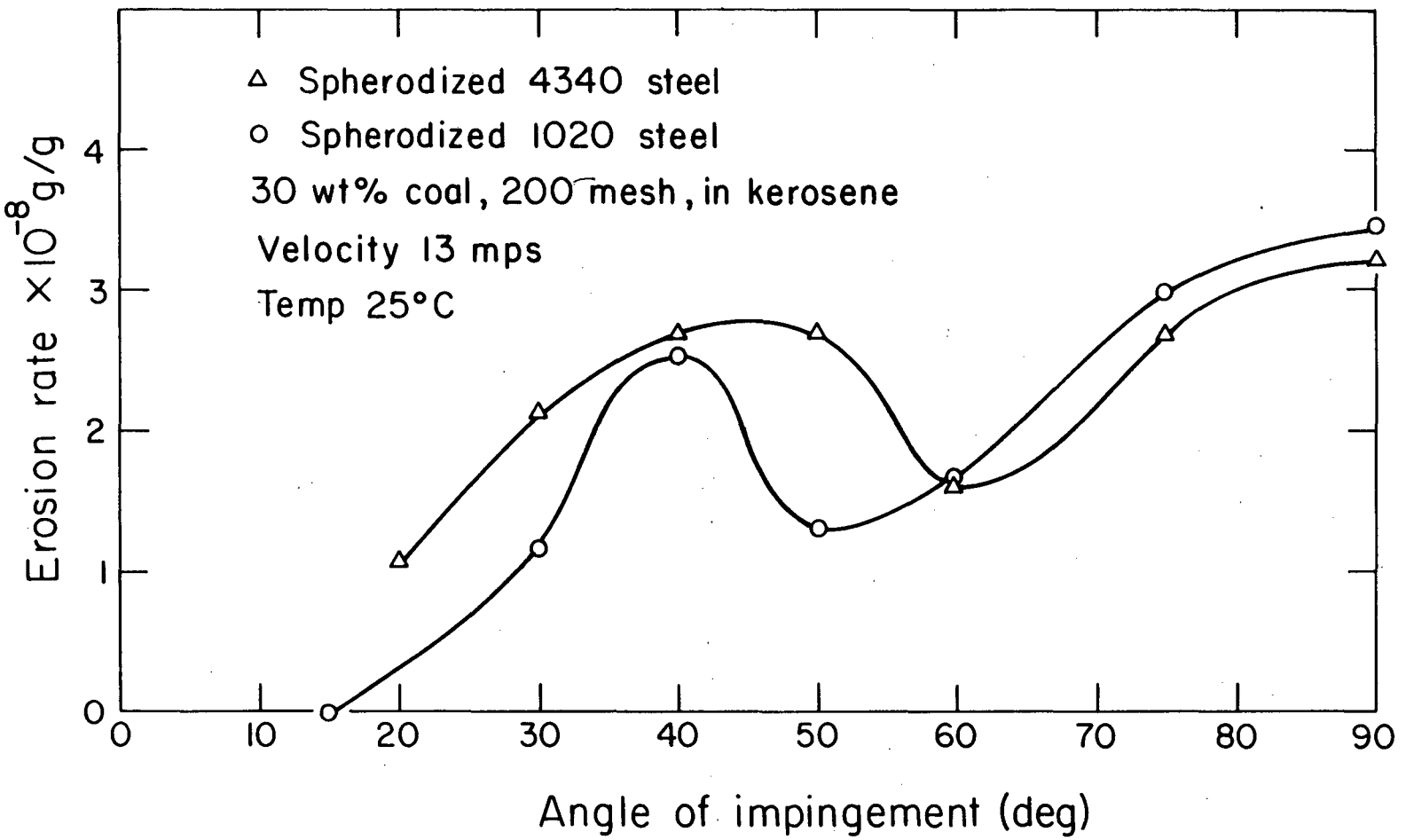

XBL 8211-7300

Fig. 10. Effect of impingement angle on erosion of speroidized 1020 and 4340 steels

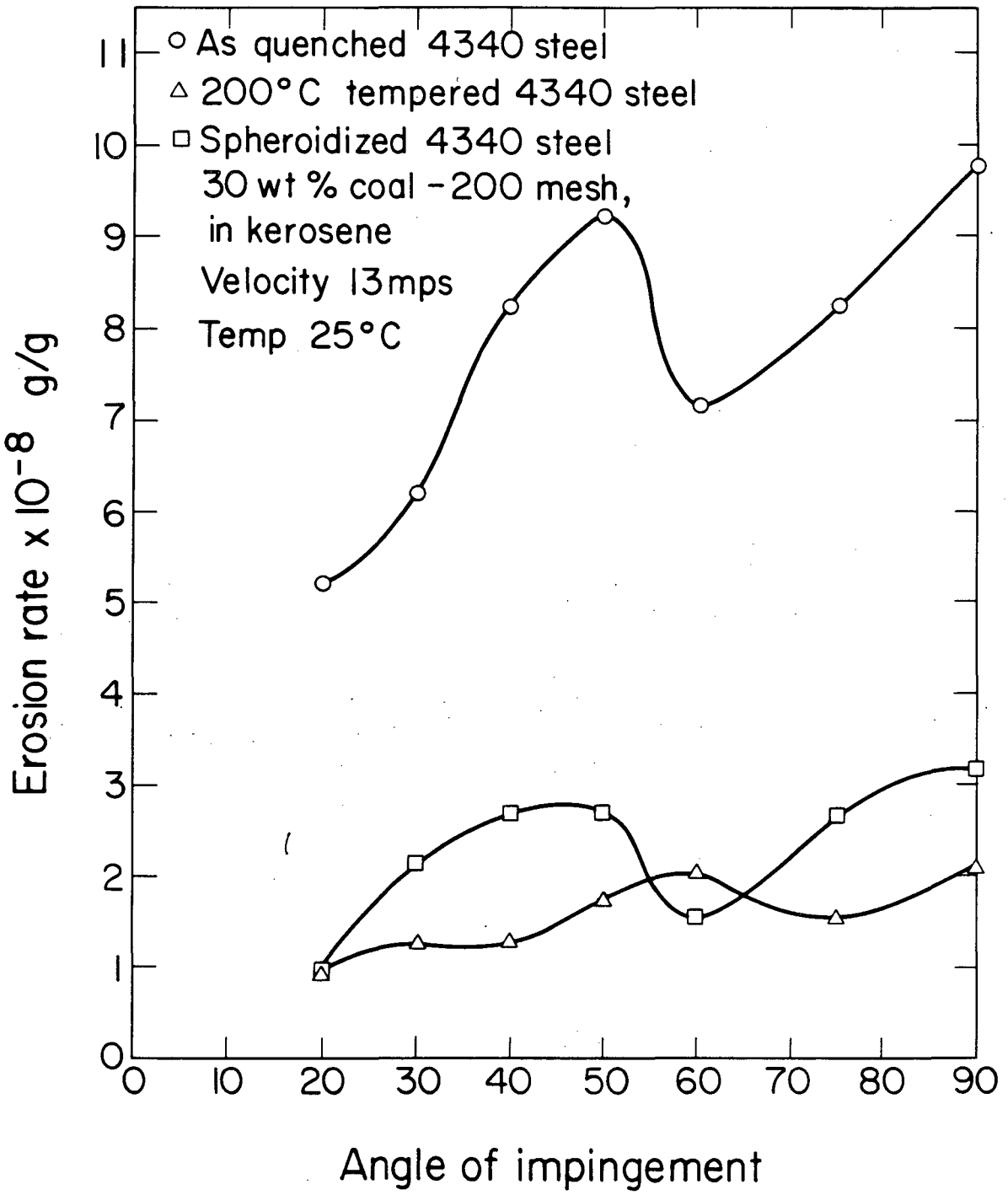

XBL 831-1074

Fig. 11. Effect of impingement angle on 4340 steel at 3 heat treatments

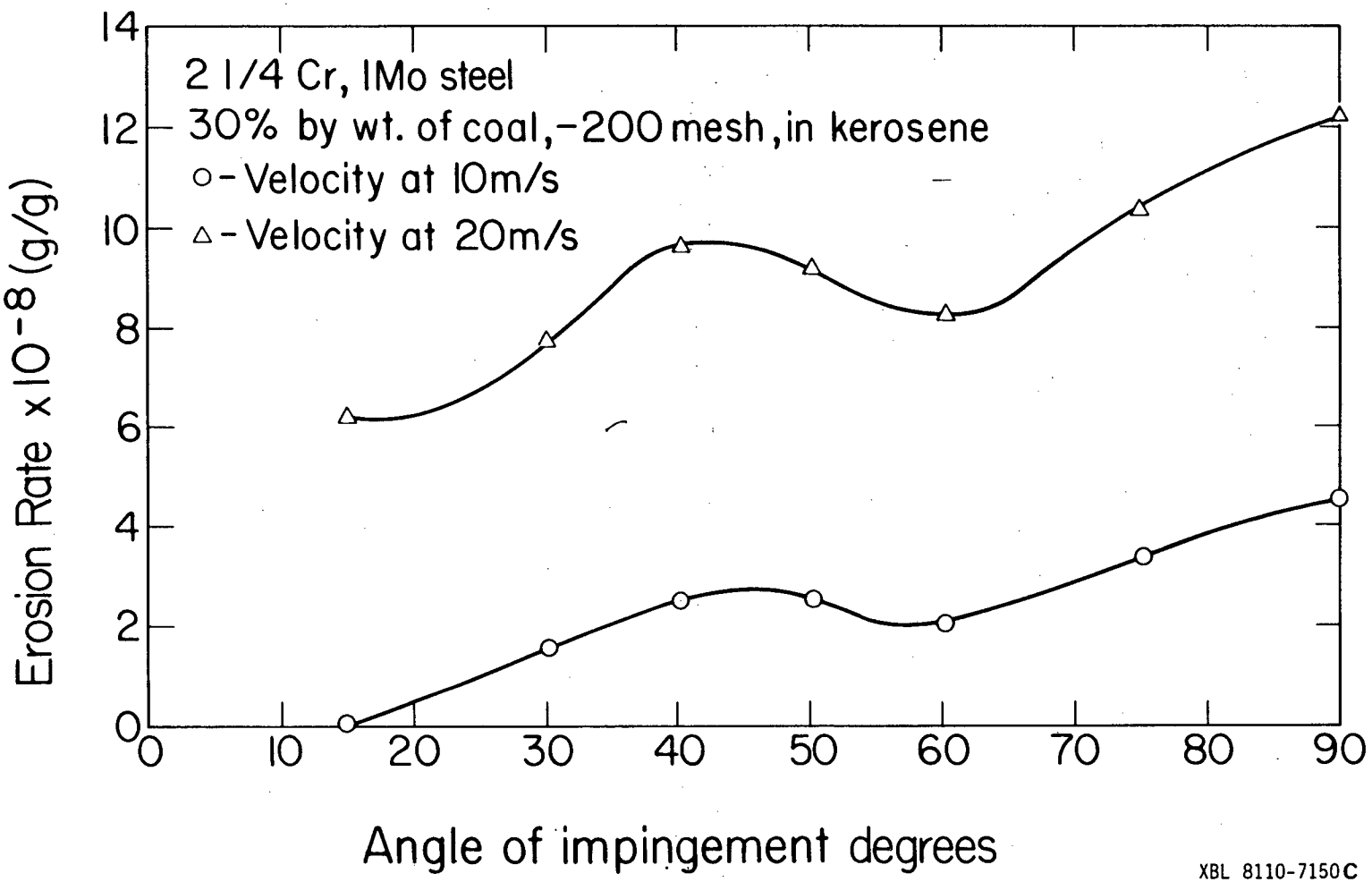

XBL 8110-7150C

Fig. 12. Effect of impingement angle on erosion of 2 1/4Cr1Mo steel

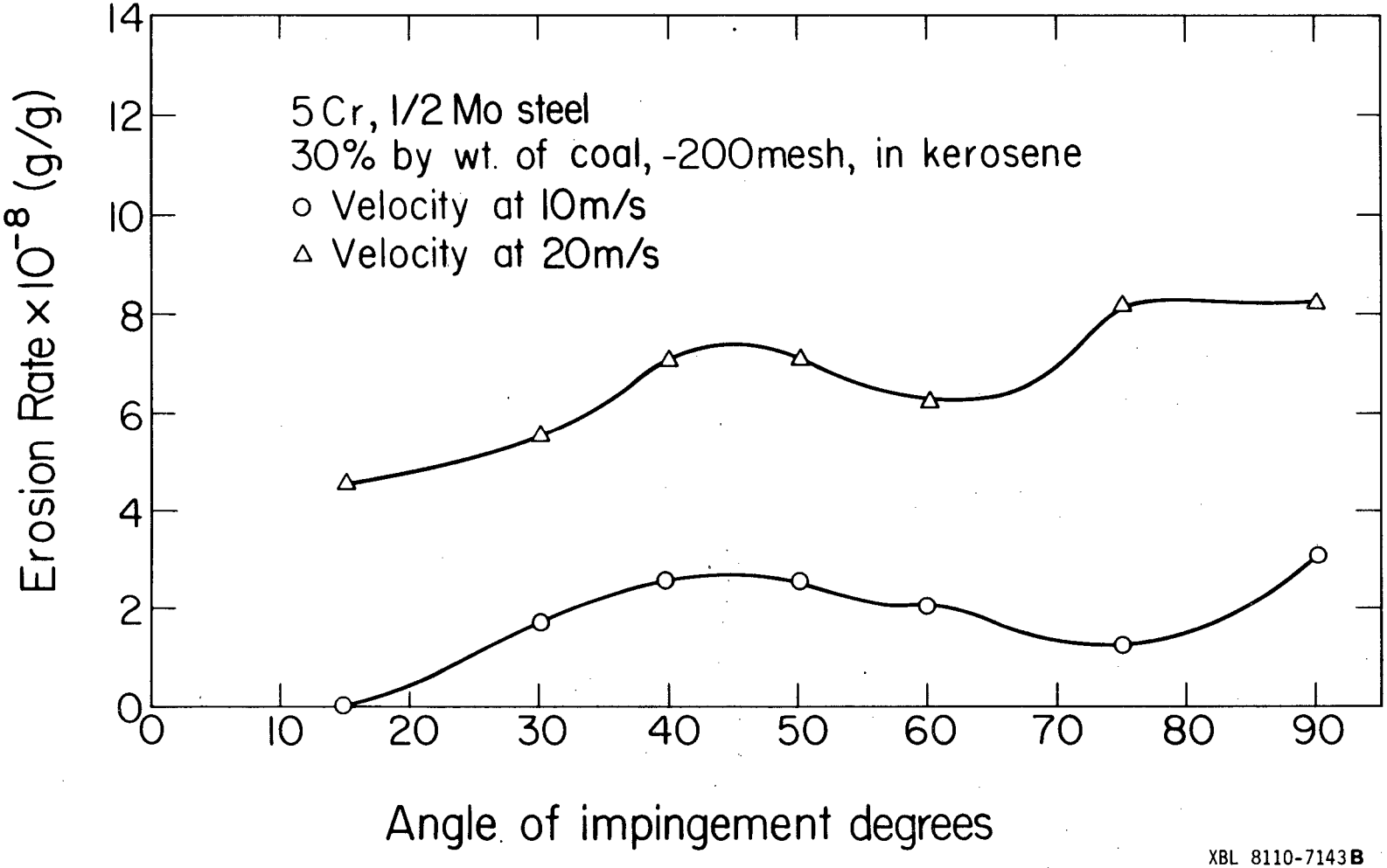

XBL 8110-7143B

Fig. 13. Effect of impingement angle on erosion of 5Cr 1/2Mo steel

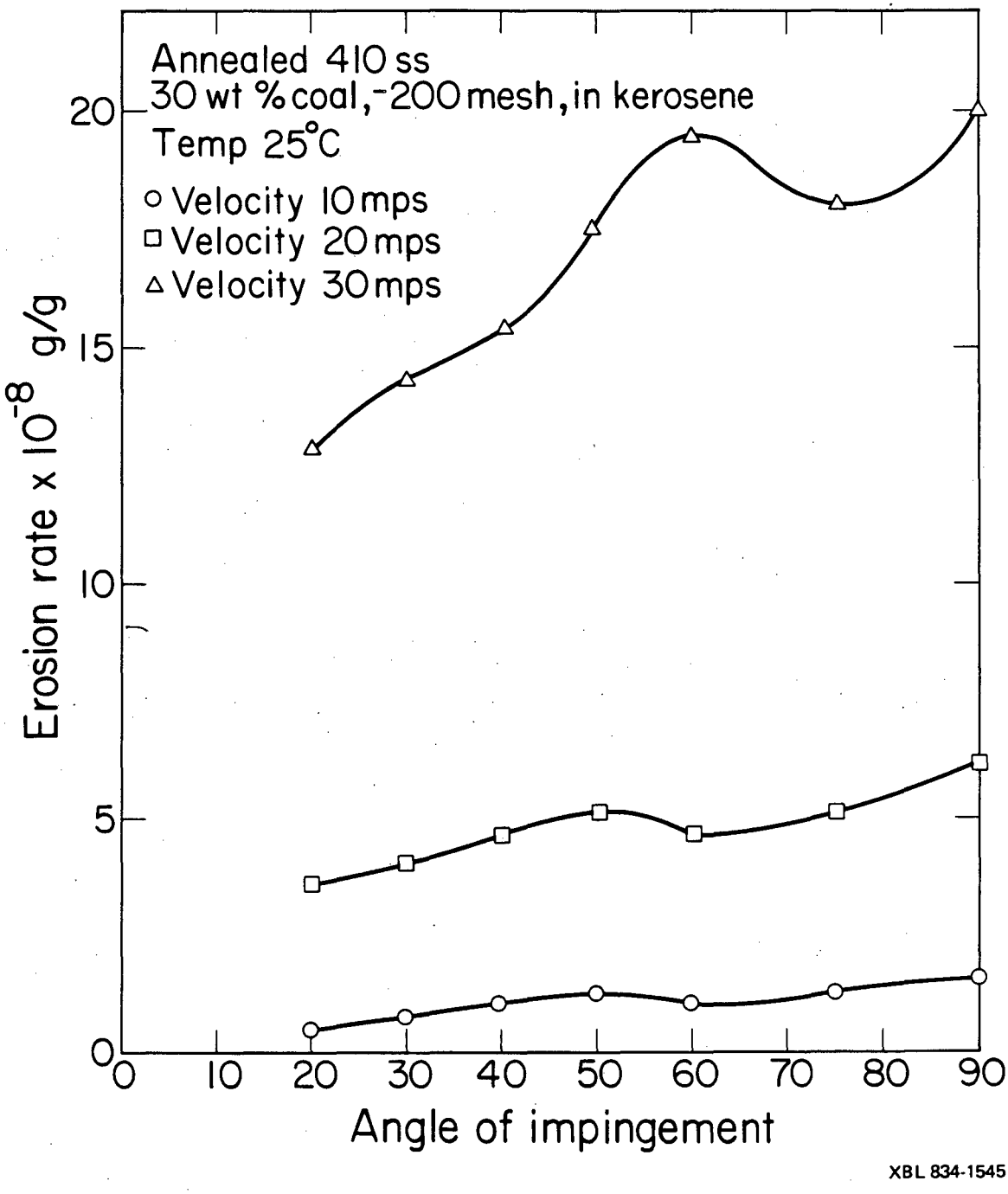

Fig. 14. Effect of impingement angle and velocity on erosion of 410SS

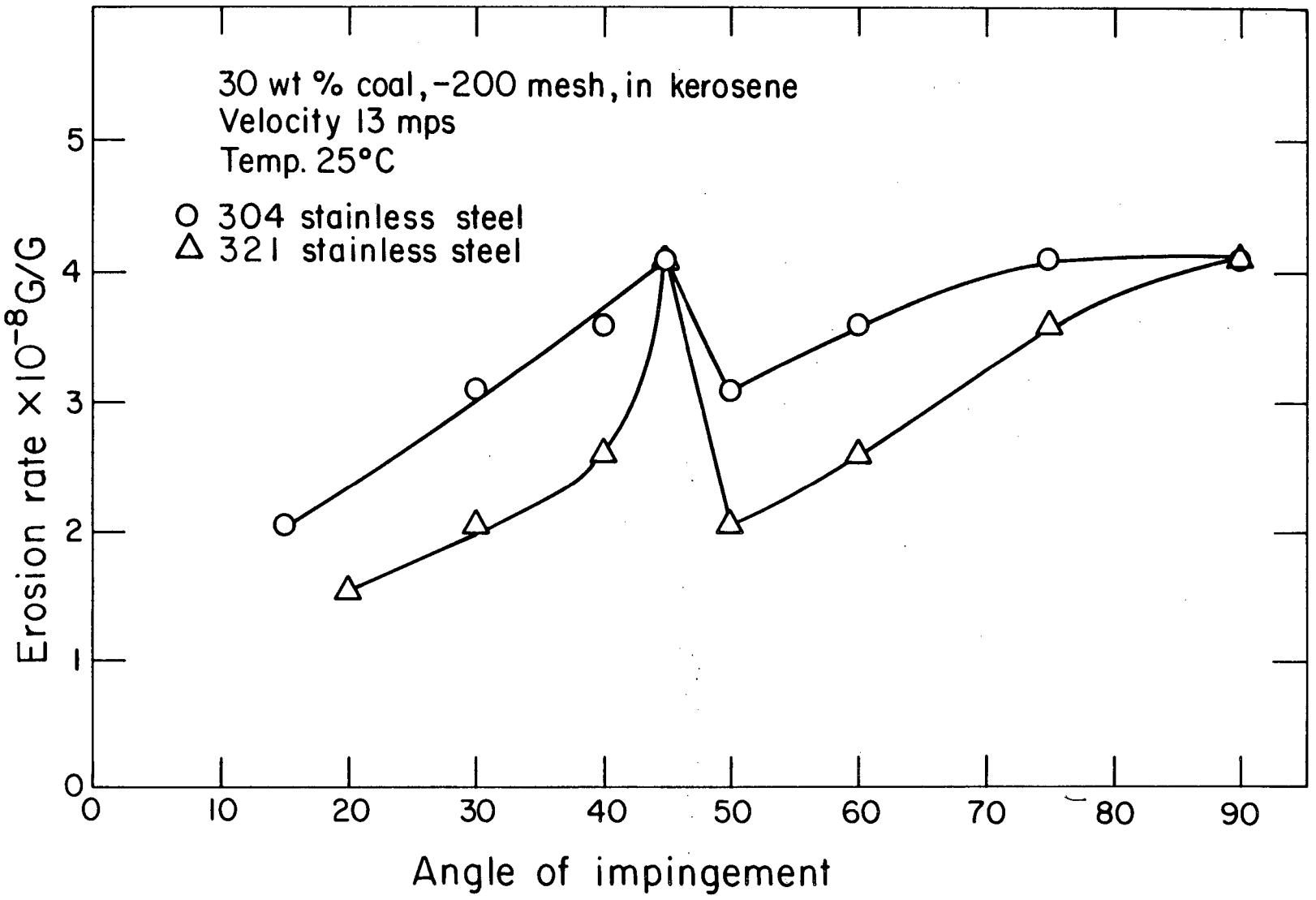

Fig. 15. Effect of impingement angle on erosion of austenitic stainless steels

XBL 834-137

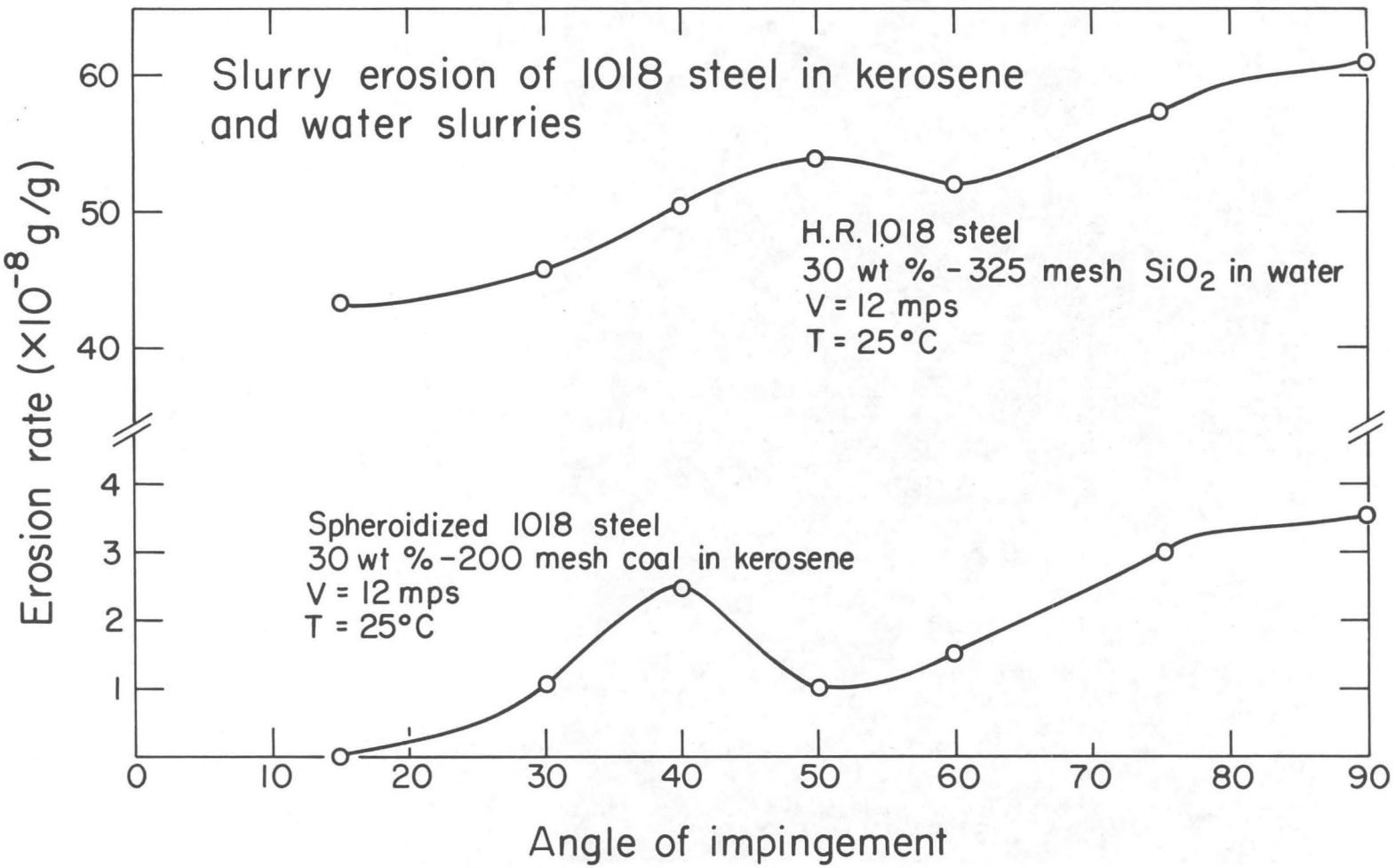

XBL 824-400

Fig. 16. Effect of impingement angle on the slurry erosion of 1018 steel from coal-kerosene and SiO_2-water slurries

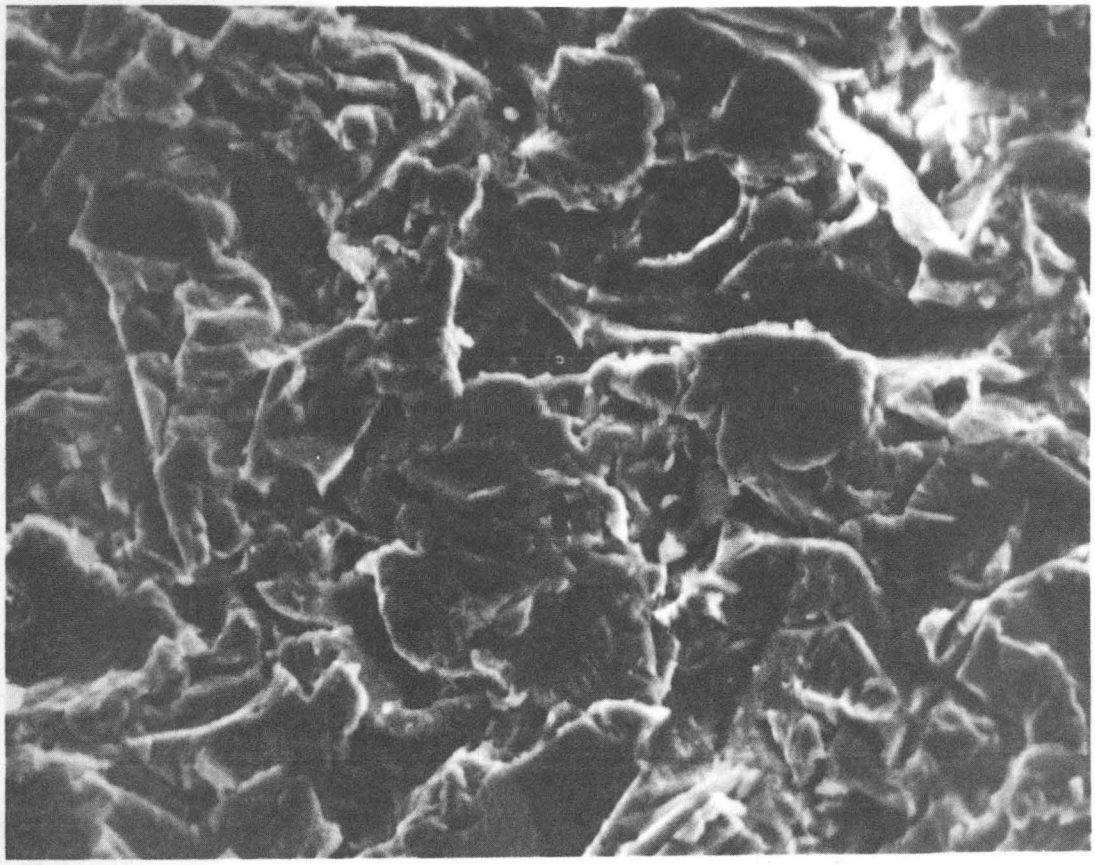

XBB 810-9318

Fig. 17. Eroded surface of 1020 steel from SiC-air test

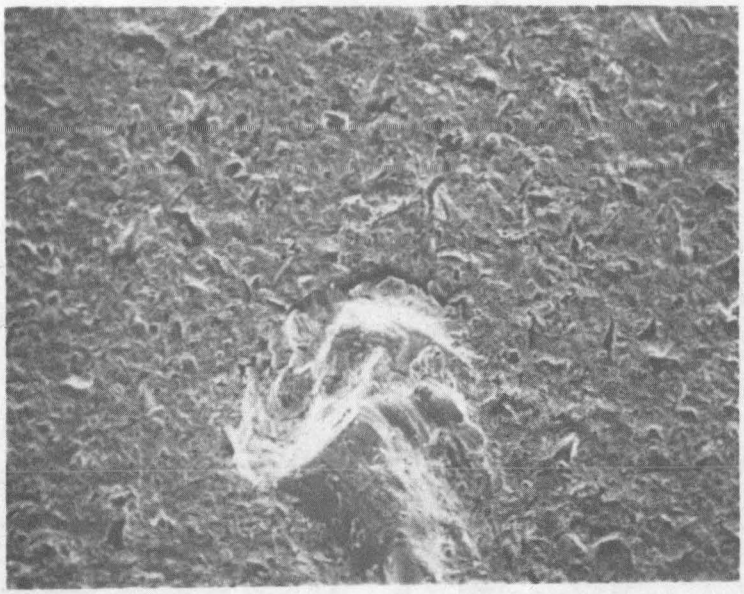

20um

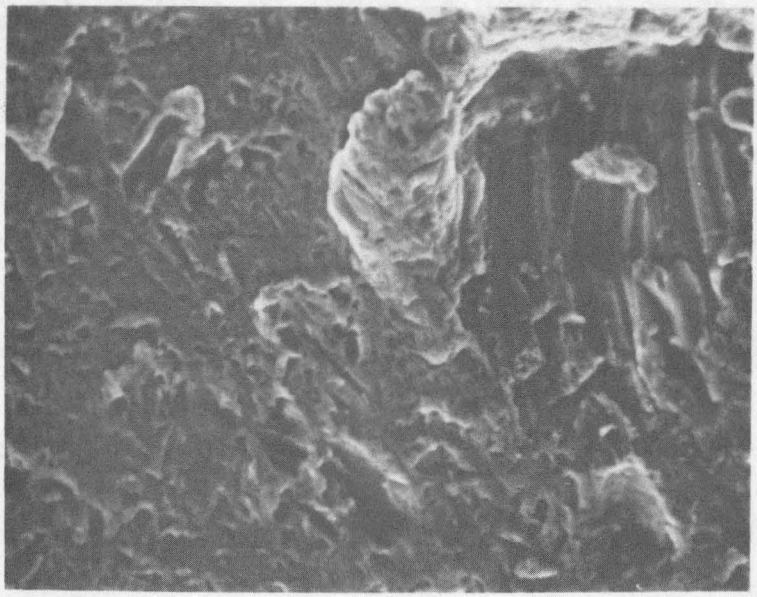

5um

XBB 819-9060

Fig. 18. Eroded surface of 1020 steel from coal-kerosene slurry test

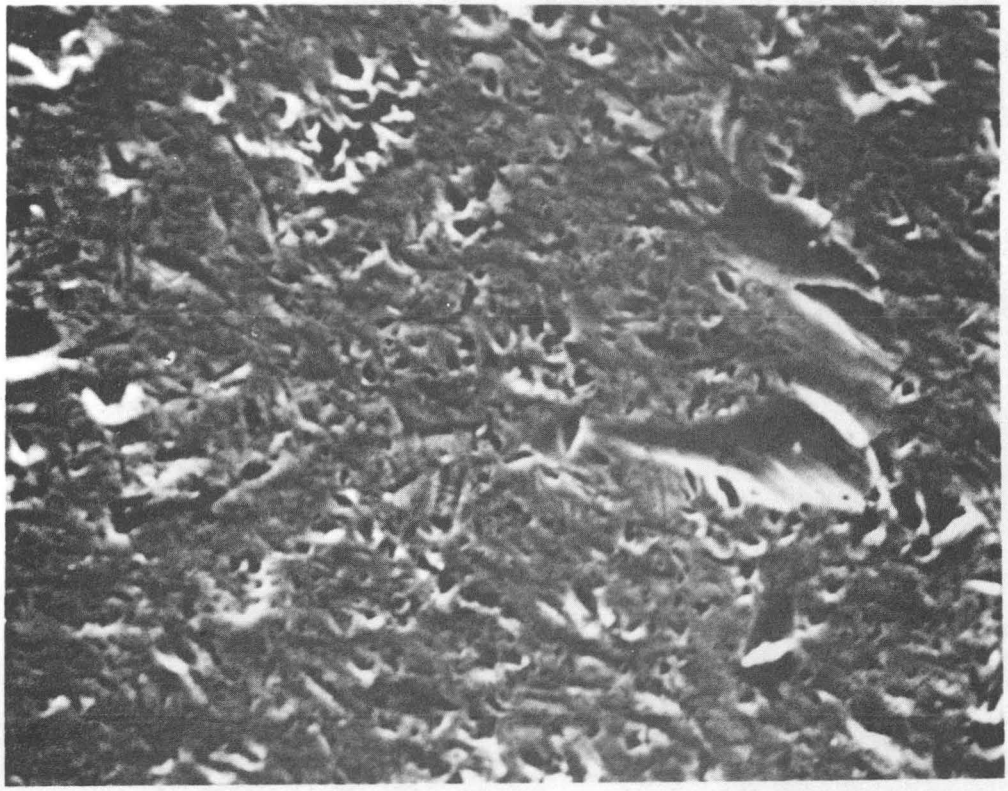

XBB 819-9061

Fig. 19. Eroded surface of 304SS from coal-kerosene slurry test

5 μm

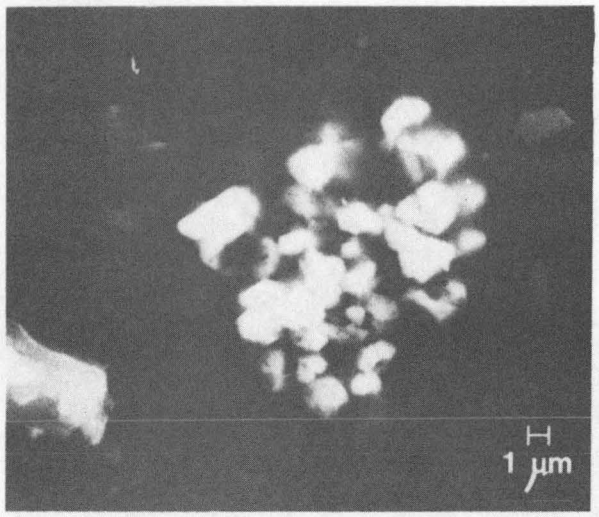

PYRITE ON
COAL SURFACE

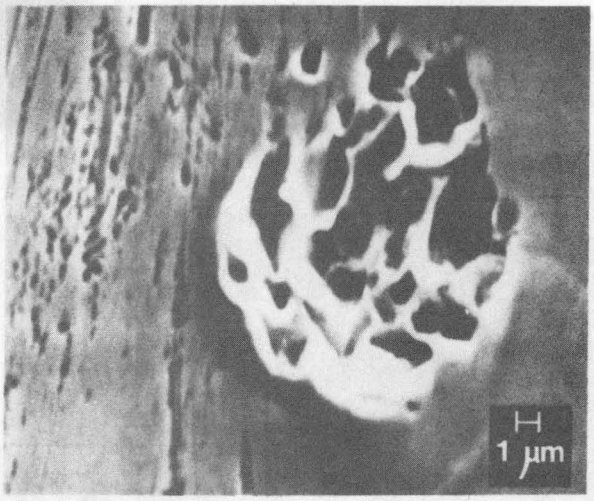

IMPRINT ON
1050 C.S. SURFACE

30° IMPACT
18 m/s

XBB 835-3893

Fig. 20. Pyrite crystallites in coal and impression in eroded steel

Fig. 21. Cross section of eroded A 53 mild steel specimen

4 μm

XBB 817-6592A

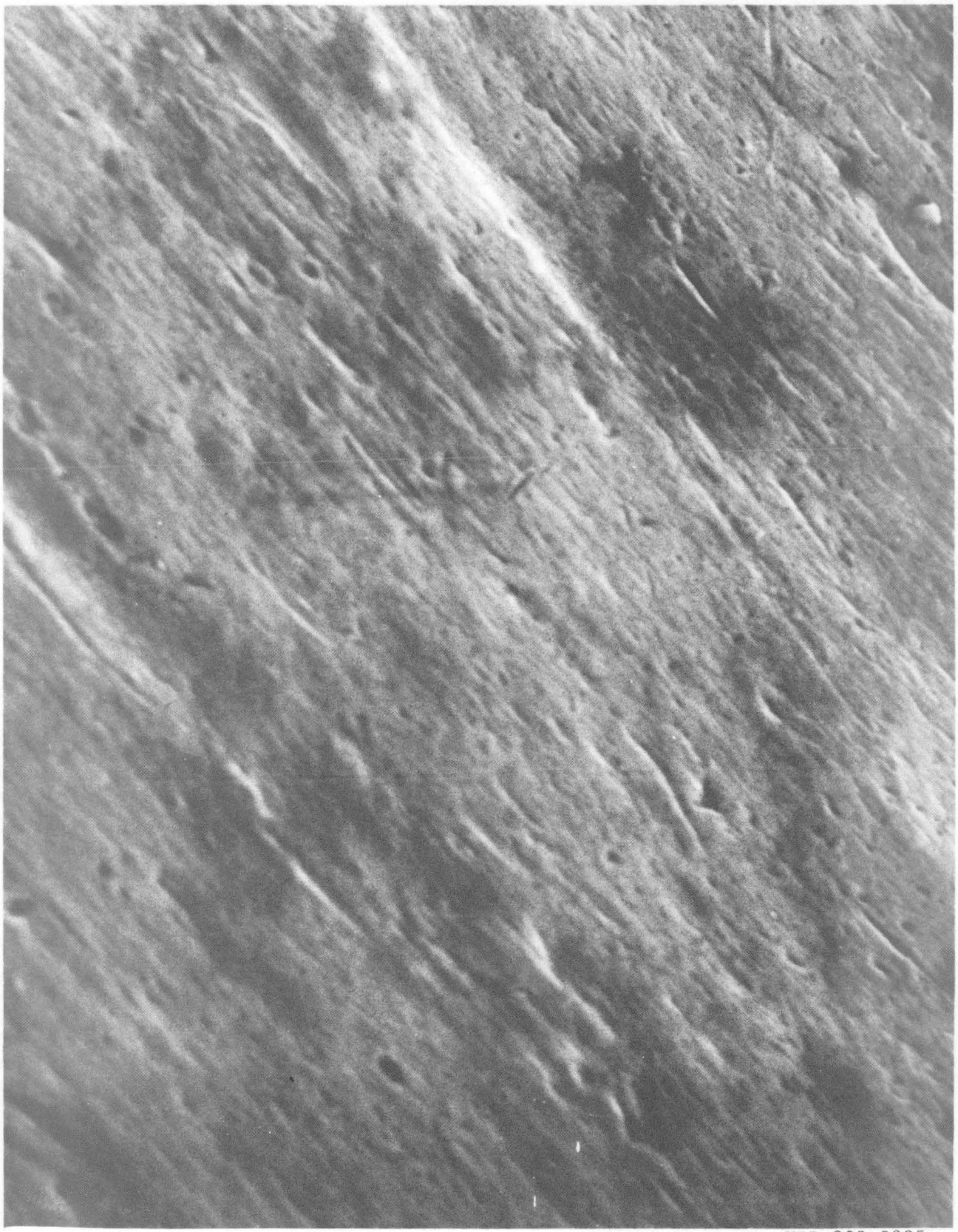

Fig. 22. Surface of eroded stainless steel elbow

XBB 802-2395

10μm

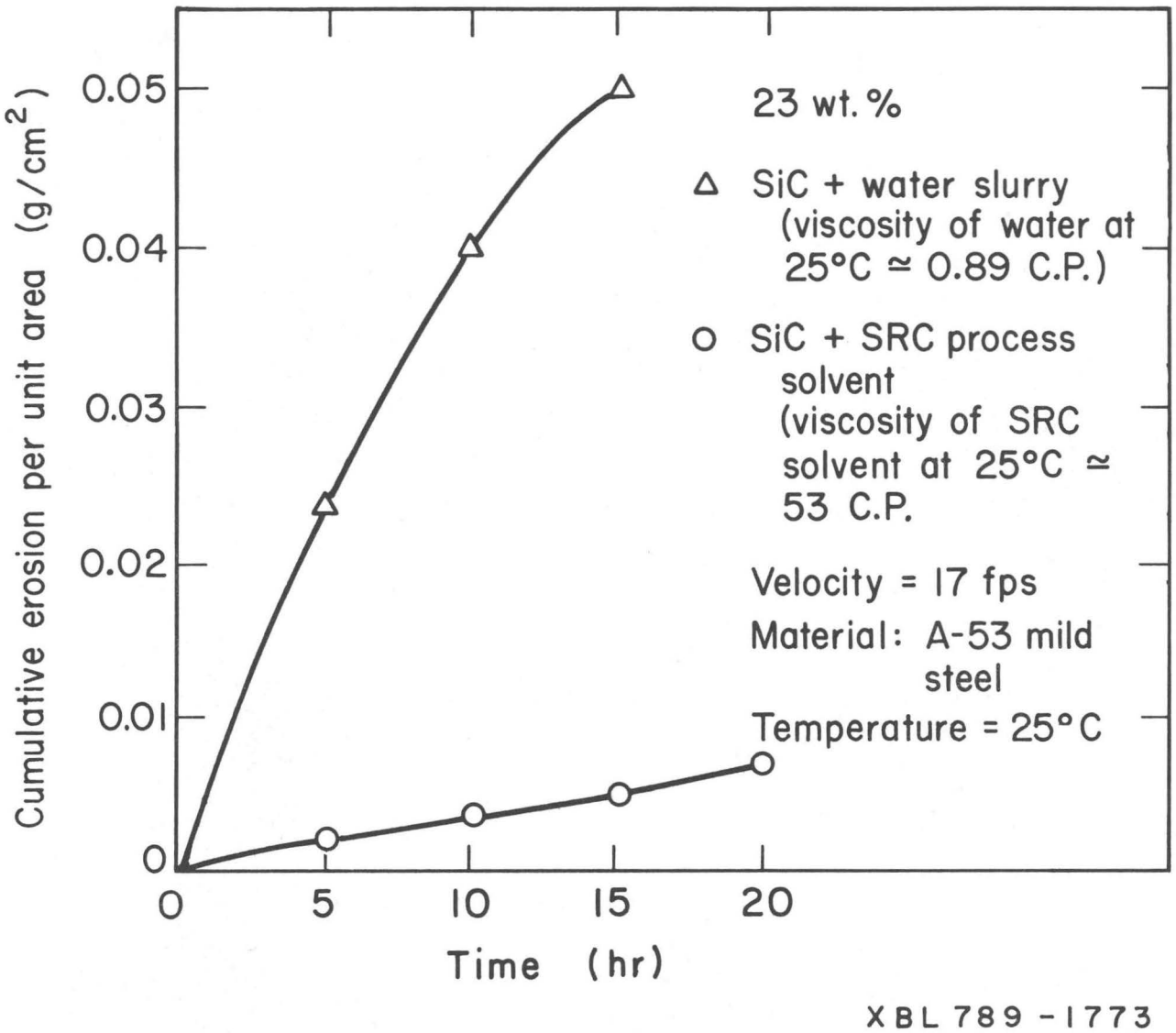

Fig. 23. Effect of viscosity on the erosion rate of A53 mild steel

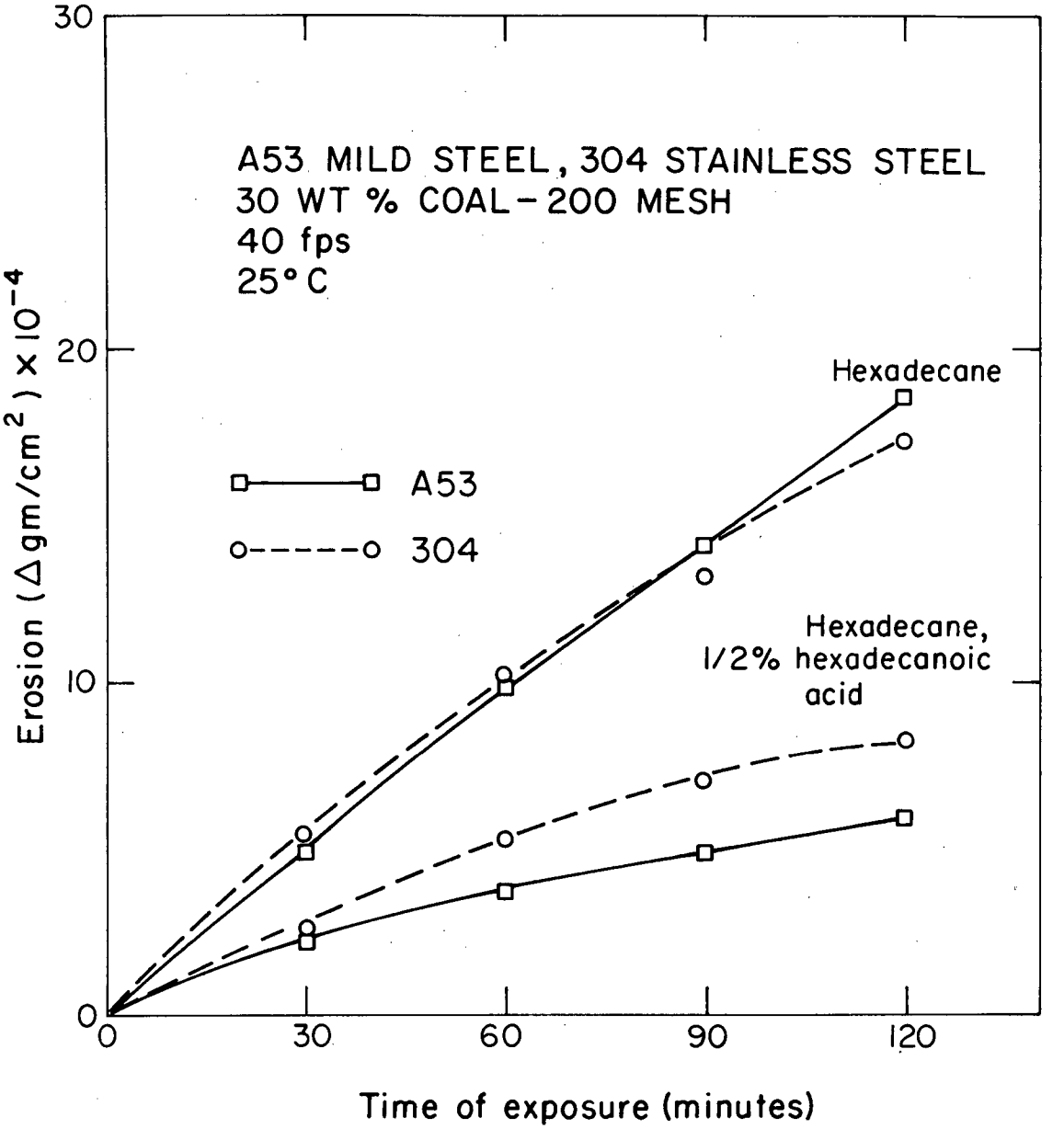

XBL 817-10721

Fig. 24. Effect of lubricity on the erosion rate of A 53 mild steel

This report was done with support from the Department of Energy. Any conclusions or opinions expressed in this report represent solely those of the author(s) and not necessarily those of The Regents of the University of California, the Lawrence Berkeley Laboratory or the Department of Energy.

Reference to a company or product name does not imply approval or recommendation of the product by the University of California or the U.S. Department of Energy to the exclusion of others that may be suitable.

TECHNICAL INFORMATION DEPARTMENT
LAWRENCE BERKELEY LABORATORY
UNIVERSITY OF CALIFORNIA
BERKELEY, CALIFORNIA 94720